iScience

CellPress
OPEN ACCESS

Article

Systematic Analysis of the Aberrances and Functional Implications of Ferroptosis in Cancer

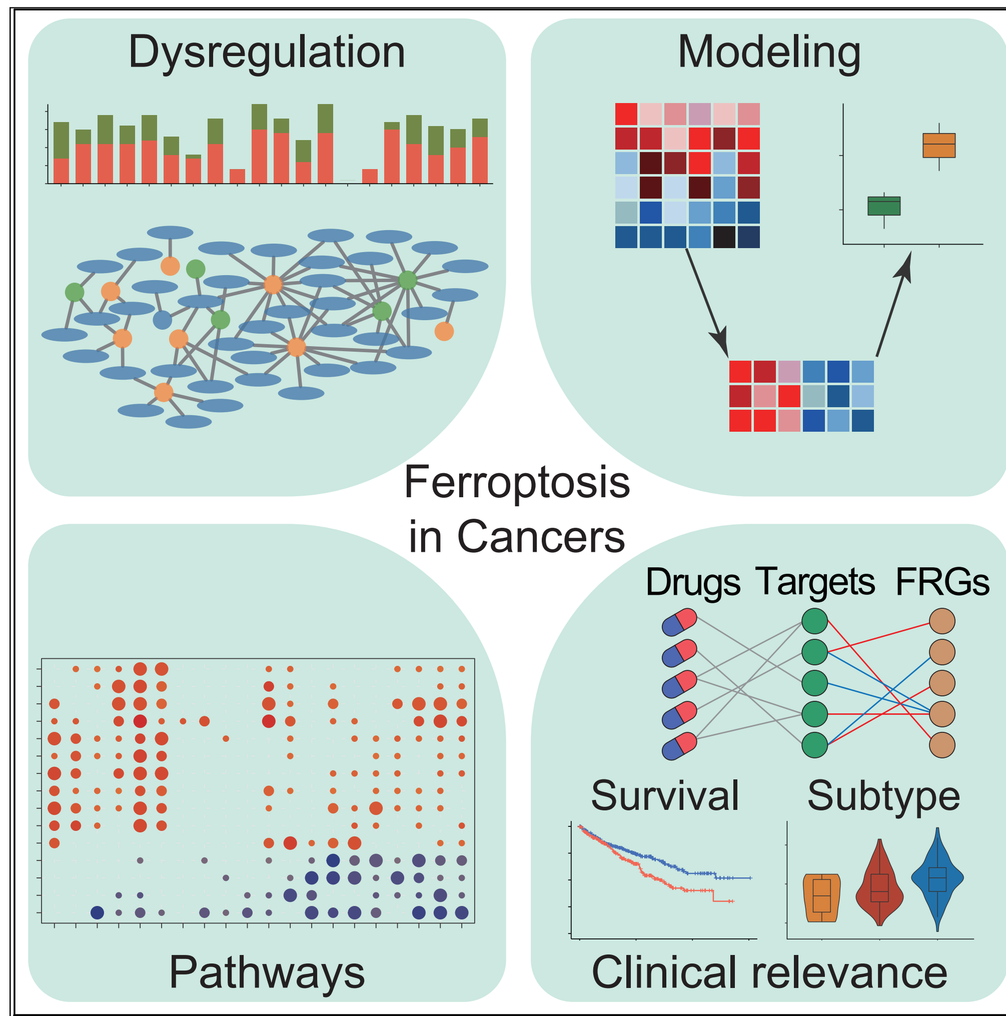

Zekun Liu, Qi Zhao, Zhi-Xiang Zuo, ..., Feng Wang, Rui-Hua Xu, Ze-Xian Liu

xurh@sysucc.org.cn (RH.X.)
liuzx@sysucc.org.cn (ZX.L.)

HIGHLIGHTS

The ferroptosis regulator genes were aberrantly expressed in tumor

The ferroptosis potential index (FPI) was established to model ferroptosis level

The FPI was correlated with metabolic, metastatic, and immune pathways

High FPI predicted poor prognosis in many cancer types

Liu et al., iScience 23, 101302
July 24, 2020 © 2020 The Author(s).
https://doi.org/10.1016/j.isci.2020.101302

iScience

CellPress OPEN ACCESS

Article

Systematic Analysis of the Aberrances and Functional Implications of Ferroptosis in Cancer

Zekun Liu,[1,4] Qi Zhao,[1,2,4] Zhi-Xiang Zuo,[1,4] Shu-Qiang Yuan,[1,4] Kai Yu,[1] Qingfeng Zhang,[1] Xiaolong Zhang,[1] Hui Sheng,[1] Huai-Qiang Ju,[1] Han Cheng,[3] Feng Wang,[1] Rui-Hua Xu,[1,2,*] and Ze-Xian Liu[1,2,5,*]

SUMMARY

Ferroptosis is a type of cell death related to cancer; however, the characteristics of ferroptosis in cancers are still uncertain. Based on the data in The Cancer Genome Atlas, we found that most ferroptosis regulator genes (FRGs) were differentially expressed in tumors, somatic copy number alterations (SCNA) and DNA methylation contributed to their aberrant expression. We established the ferroptosis potential index (FPI) to reveal the functional roles of ferroptosis and noticed that the FPI was higher in tumors than in normal tissues in most cancers and was associated with subtypes and clinical features. The FPI was negatively correlated with several metabolic pathways but positively associated with several important metastasis-related pathways and immune-related pathways. High FPI predicted poor prognosis in several tumors, whereas FPI and FRGs impacted drug sensitivity. Our study presents a systematic analysis of ferroptosis and its regulatory genes and highlights the potential of ferroptosis-based cancer therapy.

INTRODUCTION

As a newly discovered type of programmed cell death, ferroptosis results from the accumulation of iron-dependent lipid hydroperoxides and leads to cytological changes; the features and mechanisms of ferroptosis are different from those of typical cell death processes, such as apoptosis (Dixon et al., 2012). Previous studies demonstrated that, during the process of ferroptosis, sufficient and available cellular iron is required (Dixon et al., 2012). Inhibition of system X_C^-, which is a membrane Na^+-dependent cysteine-glutamate exchange transporter, and GPX4 can disrupt the oxidation-reduction balance and cause overwhelming lipid peroxidation that ultimately results in cell death (Stockwell et al., 2017; Yang et al., 2014; Yu et al., 2017). The initiation and execution of ferroptosis are affected by multiple factors, including amino acids, lipids, and iron metabolism, and are regulated by various signaling pathways, such as amino acid and glutathione metabolism, lipid metabolism, iron metabolism, and the mevalonate pathway (Stockwell et al., 2017).

As the understanding of ferroptosis has increased, its complex biological function has been revealed (Matsushita et al., 2015; Yang and Stockwell, 2016). Furthermore, ferroptosis has been found to be closely related to various human diseases including periventricular leukomalacia, Huntington's disease, and acute kidney injury (Friedmann Angeli et al., 2014; Inder et al., 2002; Linkermann et al., 2014; Skouta et al., 2014). In addition, the literature has confirmed that ferroptosis suppresses tumor growth and kills tumor cells (Yu et al., 2017) and then plays an important role in cancers such as renal cell carcinomas and liver cancer (Sun et al., 2016b; Yang et al., 2014). For example, erastin-induced ferroptosis decreases the growth of tumors formed from human colorectal cancer cells (Xie et al., 2017). Ductal pancreatic cancer cells with a mutant *KRAS* gene are more susceptible to ferroptosis than wild-type cells (Eling et al., 2015; Yu et al., 2017). Conversely, inducing tumor cell ferroptosis by small molecules has become an important strategy for the treatment of many tumors, such as hepatocellular carcinoma, kidney cancer, and pancreatic cancer (Eling et al., 2015; Louandre et al., 2013, 2015; Yang et al., 2014). In addition, changes in the gene expression of tumor cells also affect ferroptosis, and a number of genes have been confirmed to regulate ferroptosis. For example, *ACSL4* participates in the biosynthesis and remodeling of polyunsaturated fatty acid-Pes, and the downregulation of *ACSL4* increases the resistance to ferroptosis (Dixon et al., 2015; Doll et al., 2017).

[1]State Key Laboratory of Oncology in South China, Collaborative Innovation Center for Cancer Medicine, Sun Yat-sen University Cancer Center, Guangzhou 510060, China

[2]Precision Diagnosis and Treatment for Gastrointestinal Cancer, Chinese Academy of Medical Sciences, Guangzhou 510060, China

[3]School of Life Sciences, Zhengzhou University, Zhengzhou 450001, China

[4]These authors contributed equally

[5]Lead Contact

*Correspondence: xurh@sysucc.org.cn (RH.X.), liuzx@sysucc.org.cn (ZX.L.)

https://doi.org/10.1016/j.isci.2020.101302

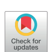

© 2020 The Author(s).
This is an open access article under the CC BY-NC-ND license (http://creativecommons.org/licenses/by-nc-nd/4.0/).

Furthermore, ferroptosis and ferroptosis regulator genes (FRGs) have been identified to be correlated with drug resistance (Lu et al., 2017). For example, it was previously reported that liver cancer cells repress ferroptosis by regulating the expression of *NRF2* or *MT-1G*, which promotes sorafenib resistance *in vitro* and in tumor xenograft models (Sun et al., 2016a, 2016b). Recently, Wang et al. reported that CD8$^+$ T cells promote tumor ferroptosis during cancer immunotherapy treatment (Wang et al., 2019). Thus, ferroptosis might play important roles during cancer progression and treatment, and a systematic study of ferroptosis and its dysregulation across cancers will be helpful.

In the present study, for the first time, we performed a comprehensive analysis of genomic variations and expression profiles of the FRGs across 20 cancer types. Furthermore, we computationally modeled the ferroptosis level based on FRGs expression and dissected the relations between ferroptosis and cancer clinical features. It was found that ferroptosis was associated with various cancer hallmarks, the immune microenvironment, drug resistance, and patient survival. These results highlight the critical roles of ferroptosis in cancer and should be helpful for further investigations of ferroptosis-related molecular mechanisms and therapy development.

RESULTS

Genetic Alterations of Ferroptosis Regulator Genes in Cancers

In this study, the twenty four genes that were identified to play critical roles in regulating ferroptosis by previous studies were defined as ferroptosis regulator genes (FRGs), including cyclin-dependent kinase inhibitor 1 (*CDKN1A*), heat shock protein family A member 5 (*HSPA5*), ER membrane protein complex subunit 2 (*TTC35/EMC2*), solute carrier family 7 member 11 (*SLC7A11*), nuclear factor, erythroid 2 like 2 (*NFE2L2*), metallothionein-1G (*MT1G*), heat shock protein beta 1 (*HSPB1*), glutathione peroxidase 4 (*GPX4*), Fanconi anemia complementation group D2 (*FANCD2*), CDGSH iron sulfur domain 1 (*CISD1*), farnesyl-diphosphate farnesyltransferase 1 (*FDFT1*), solute carrier family 1 Member 5 (*SLC1A5*), spermidine/spermine N1-acetyltransferase 1 (*SAT1*), transferrin receptor (*TFRC*), ribosomal protein L8 (*RPL8*), nuclear receptor coactivator 4 (*NCOA4*), lysophosphatidylcholine acyltransferase 3 (*LPCAT3*), glutaminase 2 (*GLS2*), dipeptidyl-dippeptidase-4 (*DPP4*), citrate synthase (*CS*), cysteinyl tRNA synthetase (*CARS*), ATP synthase, H+ transporting, mitochondrial Fo complex subunit C3 (*ATP5G3*), arachidonate 15-lipoxygenase (*ALOX15*), and acyl-CoA synthetase long-chain family member 4 (*ACSL4*) (Stockwell et al., 2017). To determine the patterns of dysregulation of FRGs in cancer, we examined the genomic data, including genetic variation, somatic copy number alternation (SCNA), mRNA expression, and DNA methylation data of tumor and normal tissues from 20 cancer types. The analysis of nonsynonymous mutations in 20 cancer types showed that the mutation frequencies for FRGs were generally low in almost all cancers and relatively high in UCEC (Figure S1A). Furthermore, *NFE2L2*, which encodes NRF2 and plays a master regulator role in antioxidant responses and has been shown to cause resistance to ferroptosis (Sun et al., 2016b), showed relatively high mutation frequencies in multiple cancers including BLCA, CESC, ESCA, HNSC, LUSC, and UCEC (Figure S1A). However, no mutations of FRGs were significantly related to survival.

To further investigate the genetic aberrations of FRGs in cancer, the percentage of SCNA was examined and the results showed that in general SCNA occurred at high frequencies (with over 5% of all samples) in most cancer types (Figure 1A), but all FRGs in THCA showed a low frequency of SCNA. FRGs presented diverse SCNA profiles. For example, *TTC35*, *HSPB1*, *TFRC*, and *RPL8* were more prone to copy number gain than copy number loss in almost all tumors, but *SCL7A11* and *ALOX15* showed the opposite profile. Furthermore, we analyzed the cooccurrence of mutations and SCNA between FRGs and cancer-specific oncogenes/tumor suppressor genes (TSGs) previously identified by Bailey et al. (2018), in which *NFE2L2* was an oncogene in cancer types including BLCA, CESC, HNSC, LIHC, LUSC, and UCEC and *CDKN1A* was a tumor suppressor gene in BLCA and LIHC. The significance was calculated via the mutual exclusivity test by DISCOVER (Canisius et al., 2016), with a false discovery rate of 1%. A total of 28 oncogenes (Figure S1B) and 43 TSGs (Figure S1C) were found to be altered with FRGs in a mutually exclusive manner in certain cancer types, and *FDFT1*, *RPL8*, *TFRC*, and *NFE2L2* were frequently exclusive to oncogenes or TSGs (Figures S1B and S1C).

Aberrant Expression of FRGs among Cancer

Besides genetic alterations, differential expression analysis was performed between tumor and adjacent normal tissues for every cancer type to investigate alterations in the gene expression patterns of FRGs, and the numbers of tumor and normal samples are shown in Table 1. We found that all FRGs were differentially expressed in at least one cancer type. Several FRGs showed consistent expression patterns in cross-cancer analysis. *SLC7A11*, *FANCD2*, *CARS*, *SLC1A5*, and *RPL8* were significantly upregulated

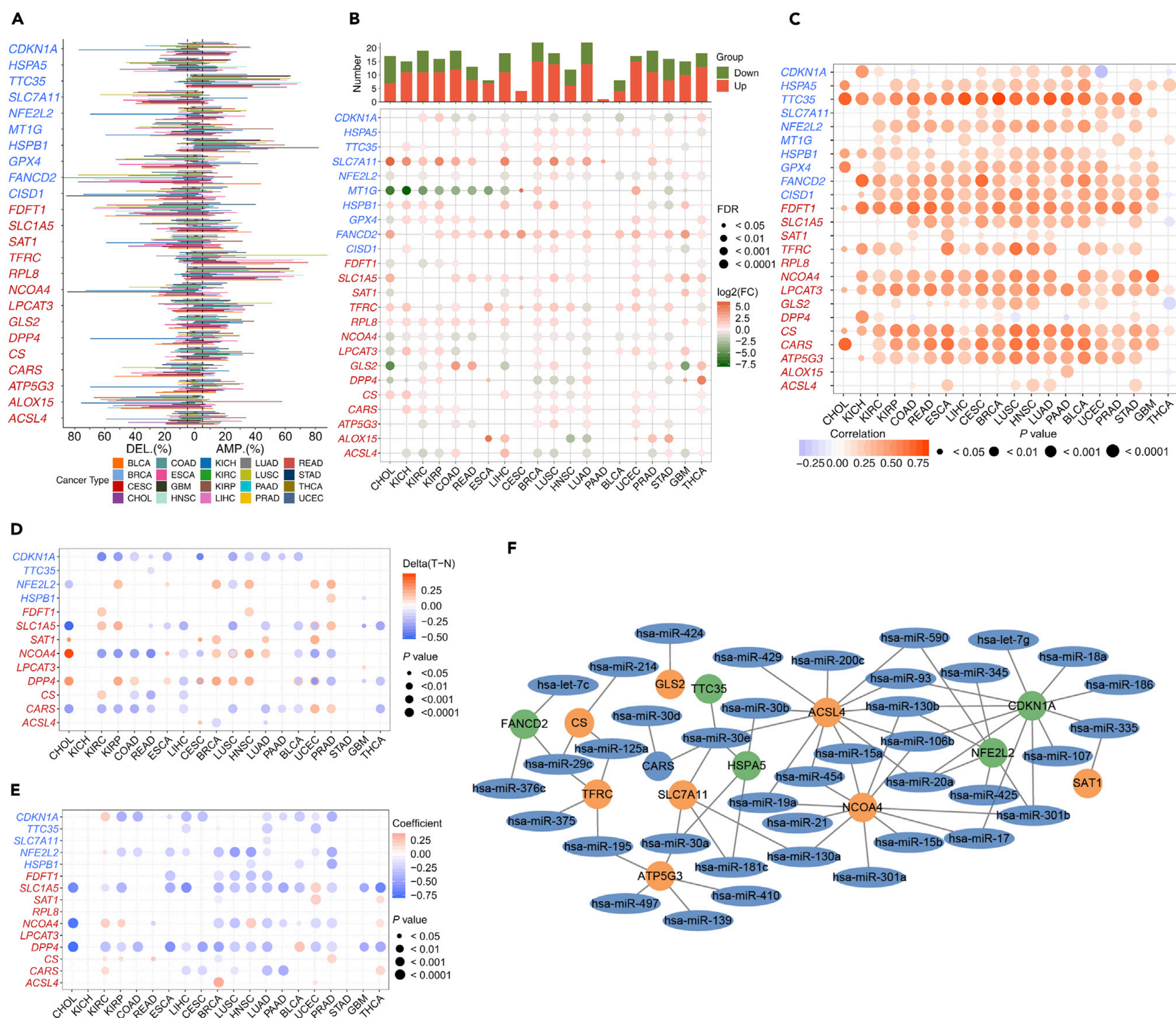

Figure 1. The Dysregulation of Ferroptosis Regulator Genes (FRGs)

For which the positive and negative regulators are marked in red and blue, respectively.

(A) Histogram shows the frequency of somatic copy number alterations for each FRG in each cancer type.

(B) Histogram (upper panel) shows the number of significantly differentially expressed genes, and the heatmap shows the fold change and FDR of FRGs in each cancer. Significantly upregulated and downregulated genes are marked in red and green, respectively.

(C) The Spearman's correlation between somatic copy number alterations and the expression of FRGs.

(D) Heatmap shows the differential methylation of FRGs in cancers; hypermethylated and hypomethylated genes are marked in red and blue, respectively (Wilcoxon rank-sum test).

(E) Pearson's correlation of FRGs between transcriptional expression and promoter methylation. Red and blue represent positive and negative correlations, respectively.

(F) The miRNA-mRNA network for FRGs, the orange and green circles are positive and negative FRGs, respectively (Spearman's Rho < -0.1, FDR <0.05).

in 15, 18, 12, 15, and 14 types of cancers, respectively, whereas *NCOA4* was downregulated in 15 cancers (Figure 1B). Additionally, several FRGs showed miscellaneous cancer type-specific patterns that have not been well characterized previously. For example, *HSPA5* was upregulated in most cancer types including breast invasive carcinoma (BRCA) (fold change [FC] = 1.87, adjusted p value = 1.42×10^{-42}) and LUAD (FC = 1.90, adjusted p value = 2.45×10^{-29}) but was significantly downregulated in THCA (FC = 0.68, adjusted p value = 2.67×10^{-7}). *DPP4*, which appears to play a suppressor role in the development of cancer (Masur et al., 2006; Pro and Dang, 2004; Wesley et al., 2005), showed significant upregulation in KIRC, KIRP, ESCA,

Tumor Type	Abbreviation	Number of Tumor Samples	Number of Normal Samples
Bladder urothelial carcinoma	BLCA	408	19
Breast invasive carcinoma	BRCA	1,100	112
Cervical and endocervical cancers	CESC	306	3
Cholangiocarcinoma	CHOL	36	9
Colon adenocarcinoma	COAD	459	41
Esophageal carcinoma	ESCA	185	11
Glioblastoma multiforme	GBM	166	5
Head and neck squamous cell carcinoma	HNSC	522	44
Kidney chromophobe	KICH	66	25
Kidney renal clear cell carcinoma	KIRC	534	72
Kidney renal papillary cell carcinoma	KIRP	291	32
Liver hepatocellular carcinoma	LIHC	373	50
Lung adenocarcinoma	LUAD	517	59
Lung squamous cell carcinoma	LUSC	501	51
Pancreatic adenocarcinoma	PAAD	179	4
Prostate adenocarcinoma	PRAD	498	52
Rectum adenocarcinoma	READ	167	10
Stomach adenocarcinoma	STAD	415	35
Thyroid carcinoma	THCA	509	59
Uterine corpus Endometrial carcinoma	UCEC	544	35

Table 1. The Abbreviations and Numbers of Samples for the 20 Types of Tumors Investigated in This Study

LUAD, GBM, and THCA, but was downregulated in CHOL, KICH, BRCA, LUSC, HNSC, and STAD. We also noticed that *DPP4* had opposite expression profiles in different subtypes of tumors in the lung and kidney. This demonstrated that FRGs might play different roles in different cancers.

Since SCNA in tumors plays a critical role in regulating gene expression, we evaluated the effects of SCNA on the gene expression of FRGs. The Pearson correlation between gene expression and copy number from the masked copy number segment of TCGA was examined. The results showed that the expression of most FRGs was obviously correlated with SCNA in most tumors (Figure 1C). For example, the expression of citrate synthase (*CS*), which participates in oxidative metabolism, was significantly associated with SCNA in all cancers. This result indicates that the aberrance of copy number for FRGs is common in most cancers and can influence gene expression.

In addition to SCNA, the methylation of promoter can regulate gene expression and aberrant DNA methylation of the promoter is associated with tumorigenesis (Shen and Laird, 2013). We observed that FRGs showed complex methylation patterns in the 20 cancer types (Figure 1D), and only *CDKN1A* consistently

showed hypomethylation in 11 tumors. For example, we observed that *DPP4* showed hypermethylation in seven cancer types and hypomethylation in four cancer types. Although there were differences in the pattern of methylation for FRGs, a negative relationship was observed between gene expression and DNA methylation overall (Figure 1E). This result demonstrated that promoter DNA methylation may regulate the expression of FRGs in tumors.

Besides SCNA and DNA methylation, microRNAs (miRNAs) can regulate gene expression and become involved in cancer development (Macfarlane and Murphy, 2010). To determine which miRNAs are involved in regulating ferroptosis, we performed an analysis to reveal the network of miRNA-FRGs. The starBase database was used to infer miRNAs that potentially target FRGs, and those miRNAs that were significantly negatively correlated with gene expression were thought to be involved in the regulation of FRGs (Li et al., 2014). As the network showed (Figure 1F), all of the interactions between miRNA and FRGs occurred in more than six cancers. It is obvious that FRGs could be targeted by miRNAs with high frequency, including *ACSL4*, *NCOA4*, and *CDKN1A* (Figure 1F). To further understand the dysregulation of the miRNA-FRG network in tumors, we conducted differential expression analysis of miRNA and quantified the expression aberrances of miRNAs across cancer types (Figure S1D). It was found that several miRNAs had consistent expression trends in tumors, for example, hsa-miR-93 targeted *CDKN1A* and was downregulated in 11 cancers. On the other hand, miRNAs had different expression trends in different tumors. For example, hsa-miR-375 targeted *ACSL4* in five tumors, but it showed upregulation in two cancers and downregulation in three cancers. This suggests that miRNAs play a regulatory role in FRGs expression, and the aberrant expression of miRNAs in tumors could impact ferroptosis.

Since SCNA, DNA methylation, and miRNA expression can all regulate FRGs expression, but their detailed contributions to gene expression are not clear. The linear regression approach was applied to analyze the contribution of each factor and diminish the confounding effects. As the results showed (Figure S1E), SCNA was positively correlated with gene expression, whereas methylation and miRNA expression showed a negative correlation. We further observed multiple regulatory patterns in FRGs, and the expression of several FRGs was only related to a single factor in several tumors, whereas others were related to multiple factors. For example, *ACSL4* expression was only associated with miRNA expression in seven cancers, including BLCA, CESC, KIRC, KIRP, LUAD, PRAD, and UCEC. SCNA played the only significant regulatory role for *CARS* in CHOL, ESCA, and colorectal cancer. However, the expression of *NCOA4* and *NFE2L2* was significantly regulated by three factors in seven and ten tumors, respectively. Thus, all FRGs show diverse regulation patterns in different cancers. This suggests that the expression regulation patterns of all FRGs were tumor specific.

Computational Modeling of the Ferroptosis Level among Cancers

To further understand the role of ferroptosis in tumorigenesis and investigate the factors or biological processes associated with ferroptosis, the ferroptosis potential index (FPI) was modeled based on the enrichment score (ES) of positive core machine components calculated by ssGSEA minus that of negative core machine components. We evaluated the FPI through three independent GEO gene expression datasets of tumor cell lines that were treated with erastin or withaferin A (WA), which were reported as inducers of ferroptosis (Dixon et al., 2012; Hassannia et al., 2018), or ferrostatin, which was identified as an inhibitor of ferroptosis (Zhang et al., 2019). The FPI was calculated for the gene expression datasets in neuroblastoma cells (GSE112384), clear cell carcinoma cells (GSE121689), and liver cancer cells (GSE104462) (Figure S2). The results showed that erastin and WA increased the FPI markedly in all three cell lines, whereas ferrostatin obviously decreased the FPI compared with the control group (Figures S2A, S2C, and S2E). Because the increases in *CHAC1* and *PTGS2* mRNA and ACSL4 protein were associated with cells undergoing ferroptosis, but these changes were not consistent in all experiments (Stockwell et al., 2017), we compared the mRNA expression of these three genes in these three cell lines. As the results showed, the mRNA expression of *PTGS2* could not significantly distinguish the ferroptosis status in these experiments. For *ACSL4*, there were no obvious changes in cell lines with ferroptosis induced by erastin or WA, although decrease was observed in the ferroptosis-inhibited cells (Figures S2B and S2D). *CHAC1* was upregulated in ferroptosis-induced cell lines treated with erastin or WA but only slightly upregulated in ferroptosis-inhibited cells (Figure S2F). Thus, the FPI could be used to represent the potential level of ferroptosis based on the transcriptome data.

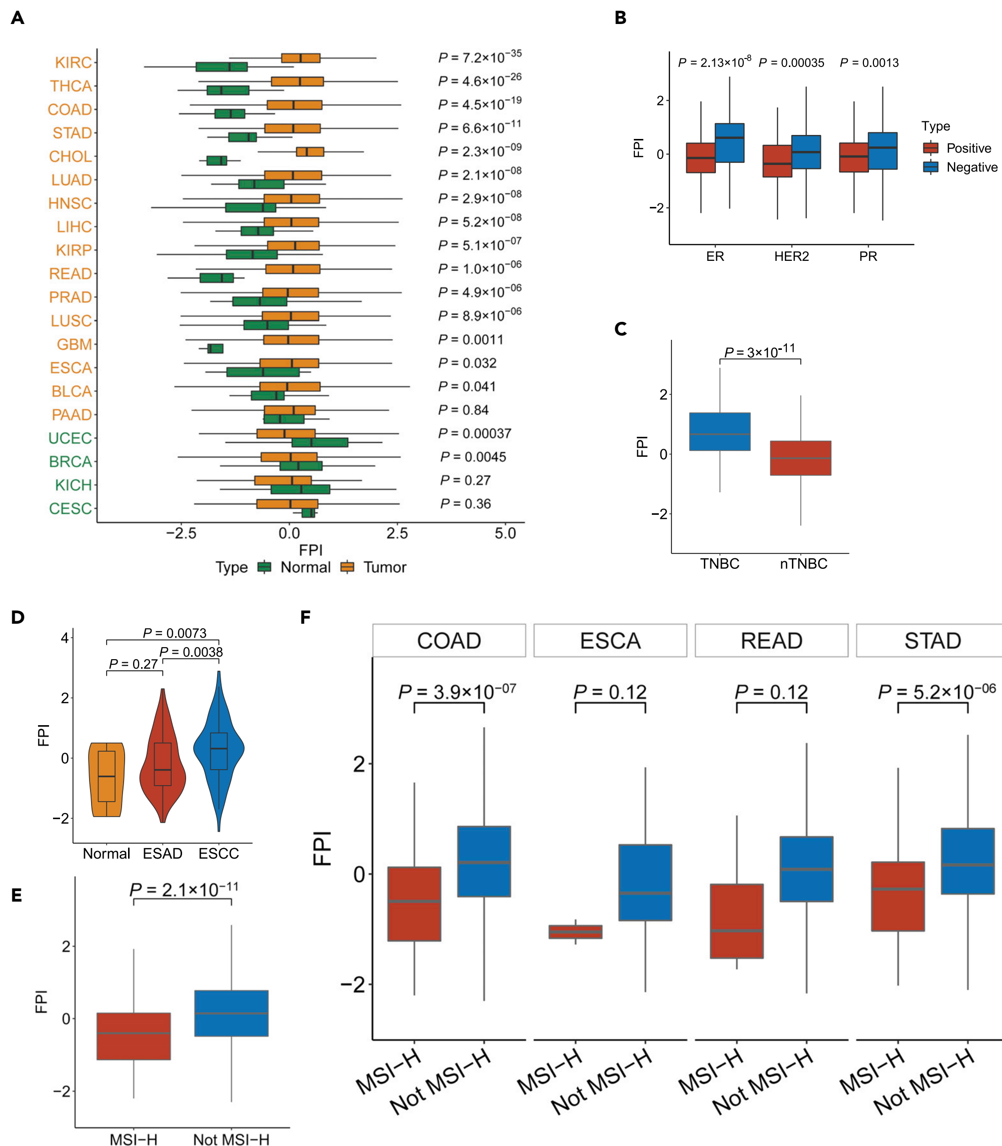

Figure 2. The Relations between FPI and Histological Types and Molecular Subtypes among Cancers

(A) The different FPIs between tumor and normal tissues among cancers.

(B) Box shows the difference of in FPI between positive and negative receptors in breast cancer.

(C) The difference in FPI between TNBC and nTNBC.

(D) The different FPIs among different histological types of esophageal carcinoma.

(E and F) The FPI for different MSI statuses of overall (E) and detailed (F) digestive system neoplasms. The boxes in (B)–(F) mean the median values ± 1 quartile, their whiskers extending from the hinge to the smallest or biggest value, which is $1.5 \times$ interquartile range (IQR) from the box boundaries. All tests were Wilcoxon rank-sum test.

Next, we compared the differences in FPI, the computed marker of ferroptosis, between tumor and normal tissues with the cancer genome atlas (TCGA) data (Figure 2A). Of note, significant differences were found in most cancers such as lung cancer and gastrointestinal cancer and higher FPI was observed in most tumors except for BRCA and UCEC. We also noticed that the FPI of normal tissues in female cancers (BRCA, UCEC, and CESC) was higher than most tumor/normal samples in all cancers. To further dissect the factors involved in these different FPI patterns, we examined the FPI for different subtypes of BRCA. The results presented in Figure 2B showed that all estrogen receptor (ER)-positive, progesterone receptor (PR)-positive, and HER2-positive patients had lower FPIs than the negative patients. Furthermore, triple-negative breast cancer (TNBC) samples showed higher ferroptosis levels than non-TNBC samples (Figure 2C), which

CellPress
OPEN ACCESS

was consistent with a previous study (Kettner et al., 2016). Furthermore, among the different subtypes of kidney cancer, the FPI of tumor samples was higher than normal in KIRP and KIRC, whereas the FPI in KICH was lower (Figure 2A). In addition, to further dissect the variances of ferroptosis levels in different histological types, the FPIs in esophageal squamous cell carcinoma (ESCC) and esophagus adenocarcinoma (ESAD) were compared. The results showed that the FPI in ESCC was significantly higher than in ESAD and normal samples, whereas the FPI in ESAD was higher than that in normal but not significant (Figure 2D).

In addition to the cancer types and subtypes, we analyzed the correlation between the FPI and remarkable molecular features such as microsatellite instability (MSI) and driver gene mutations. The FPI decreased obviously in tumors with a high level of MSI (MSI-H) compared with non-MSI-H tumors in gastrointestinal tumors (Figure 2E). The FPI was markedly lower in patients with COAD and STAD with MSI-H, and a slight decrease was also observed in ESCA and READ (Figure 2F). Furthermore, we analyzed the correlation between FPI and 375 driver genes that are frequently mutated in tumors based on regression-based analysis. By controlling for cancer type and tumor mutation burden (TMB), 81 genes were found to be correlated, and most of them were negatively associated with FPI (adj.p < 0.1, Figure S3A). Strikingly, somatic mutations, namely, *NFE2L2*, *BRAF*, and *TP53*, were positively associated with FPI in pancancer associations, but a mutation in *TP53* was negatively correlated with ferroptosis in LUSC. This observation was verified by the comparison of FPI between the *TP53* mutant and wild-type groups (Figure S3B), consistent with previous findings that showed that *TP53* played a dual role in regulating ferroptosis (Kang et al., 2019). The influences of *KRAS* mutations on FPI were also investigated, and the results showed that the relationship between *KRAS* mutation and FPI was significantly negative in gastric tumors (Figure S3C) but slightly positive in hepatocellular carcinoma (Figures S3A and S3C). These results indicated that the tumor type and molecular context were critical for the regulation of ferroptosis, which was consistent with a previous study (Tsoi et al., 2018). Furthermore, differential expression of FRGs between wild-type and tumors with mutant *TP53* (Figure S3D) and *KRAS* (Figure S3E) was found to be ubiquitous in most cancers. Taken together, these data indicate that ferroptosis is negatively related to MSI-H in cancer.

Association between Ferroptosis and Pathways in Cancer

To further elucidate the association between the FPI and other genes and pathways, we calculated Spearman correlation coefficients between FPI and all the genes including FRGs (Table S1). It was found that FPI was generally positively and negatively correlated with the expression of positive and negative FRGs, respectively, but various exceptions were also observed (Table S1). The related cellular signaling of ferroptosis in cancer was investigated by gene set enrichment analysis (GSEA) for each cancer based on the transcriptome of two tumor groups with the top and bottom 30% of FPI. It was observed that metabolism-related pathways in KEGG were usually enriched in tumors with lower FPIs, and pathways frequently enriched (>6 cancers) are presented in Figure 3A. For example, terpenoid backbone biosynthesis and steroid biosynthesis were enriched in the low-FPI group in 19 and 16 cancers, respectively (Figure 3A). Peroxisome, biosynthesis of unsaturated fatty acids, etc. were also significantly correlated with lower FPI in all these cancer types (Figure 3A). Furthermore, the relations between cancer hallmarks and FPI were also analyzed, and the results showed that 15 hallmarks were frequently significantly correlated with FPI (Figure 3B). For example, KRAS signaling, epithelial-mesenchymal transition, IL6 JAK STAT3 signaling, and WNT Beta-catenin signaling were enriched in the high-FPI group, which indicated that ferroptosis was positively related to these oncogenic pathways (Figure 3B). Additionally, metabolism-related hallmarks were observed to be negatively related to ferroptosis, which was consistent with the pathway analysis (Figure 3B).

Since previous studies showed that ferroptosis was related to the immune response process (Matsushita et al., 2015), we investigated the association between ferroptosis and the immune microenvironment in tumors. The results showed that, in several cancers, FPI was weakly negatively correlated with immunophenoscore (IPS) (Figure 3C), which could predict the response of the immune checkpoint blockade in melanoma tissue (Charoentong et al., 2017). To better understand the relationship between ferroptosis and the response to immunotherapy, we calculated the Spearman coefficients and found that the FPI was positively correlated with the dysfunction score of T cells in 13 cancers. However, no consistent effect of the FPI on the exclusion score of T cells was observed (Figure 3D). Furthermore, FPI was positively correlated with MHC and effector cells (ECs) but negatively correlated with immunomodulators (CP) and suppressor cells (SCs) in most cancers (Figure 3C). The associations between ferroptosis and immune cell types were further evaluated in detail, and the results showed that FPI showed a positive correlation with macrophages in most

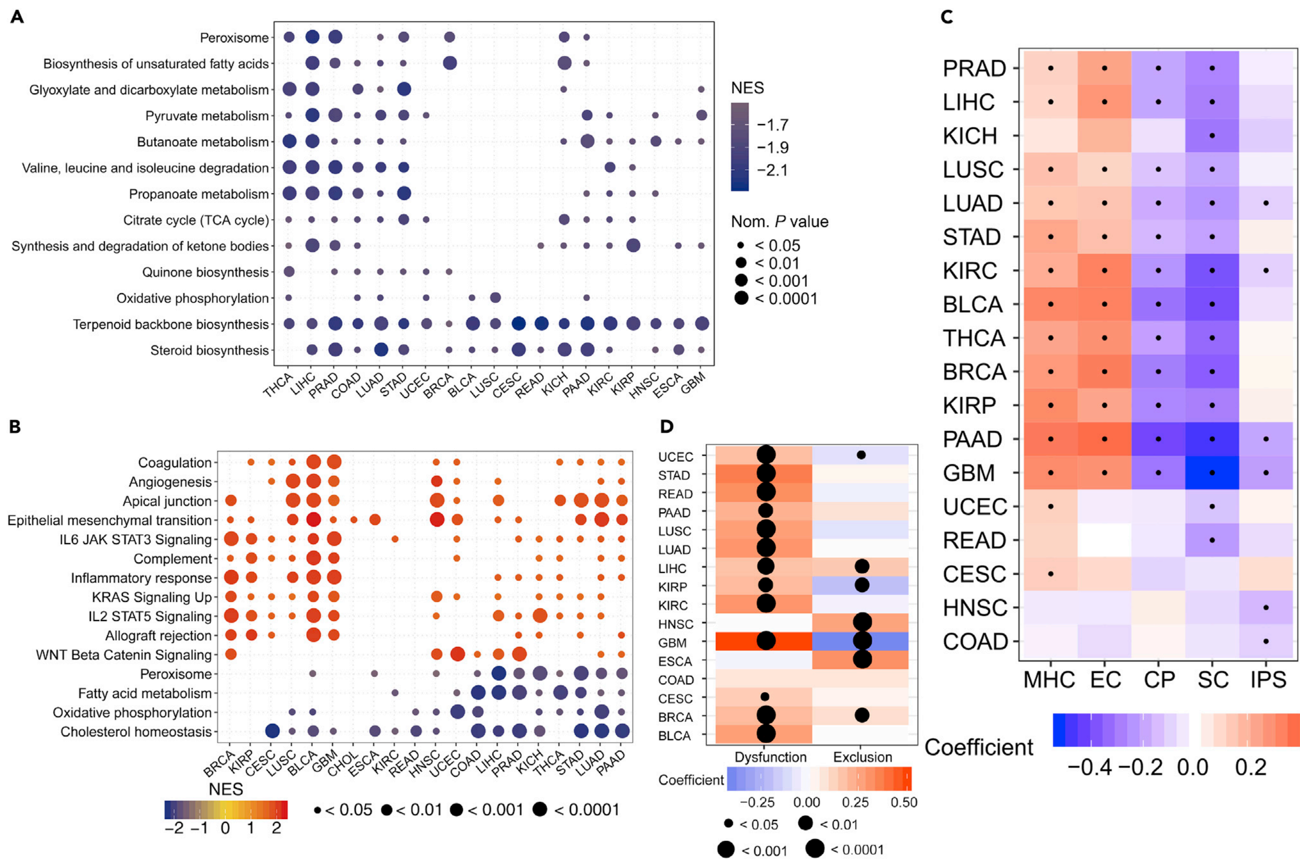

Figure 3. Relationships between Ferroptosis and Signaling Pathways and Immunophenotypes

(A and B) Enrichment analysis for metabolism pathway (A) and cancer signaling (B) between high- and low-FPI tumor tissues. NES is the normalized enrichment score in the GSEA algorithm.

(C) The Spearman's correlations between immunophenotypes and the FPI, and dots indicate statistically significant results (p value <0.05).

(D) The Spearman's rank correlation coefficient between the FPI and dysfunction/exclusion scores inferred by TIDE.

cancers and a negative association with activated dendritic cells, activated mast cells, plasma cells, and T follicular helper cells (Figure S3F). Thus, there might be close connections between ferroptosis and the immune microenvironment and the function of T cells, and more investigations are needed to reveal the details.

Clinical Relevance of Ferroptosis and Its Regulators

Since ferroptosis is involved in cellular metabolism and the immune microenvironment, it was proposed that ferroptosis and its regulators should be correlated with cancer survival and other clinical characteristics. Based on the clinical data from TCGA, survival analysis was performed and the results were consistent since it was found that the lower FPI predicted a better survival in five cancers including GBM, KIRC, KIRP, LIHC, and LUAD (Figure 4). We further dissected the factors that might impact FPI, including tumor stage, cigarette smoking, age, and sex. As shown in Figure S3G, tumor stages were positively correlated with FPI in LIHC, KIRC, KIRP, and COAD. Only the FPI in LUAD tumors showed a positive correlation with cigarettes smoked per day. Age was positively associated with FPI in GBM and PRAD but showed a negative correlation in seven cancers such as BRCA and LIHC. It was observed that FPI was markedly different between sexes (Figure S3H), FPI for female tumor samples was higher than for male tumor samples in KIRC, LIHC, LUAD, and LUSC but lower in STAD. Significant differences in FPI were also observed among different races in BLCA, BRCA, and ESCA. Furthermore, we found that the FPI was correlated with cancer metastasis, recurrence, and primary and follow-up outcome in several cancers. In addition, we evaluated the association between FPI and other clinical characteristics including alcohol abuse, fatty liver, hemochromatosis, and viral infection (HPV, HBC, HCV, and EBV), but no significant results were observed. These results

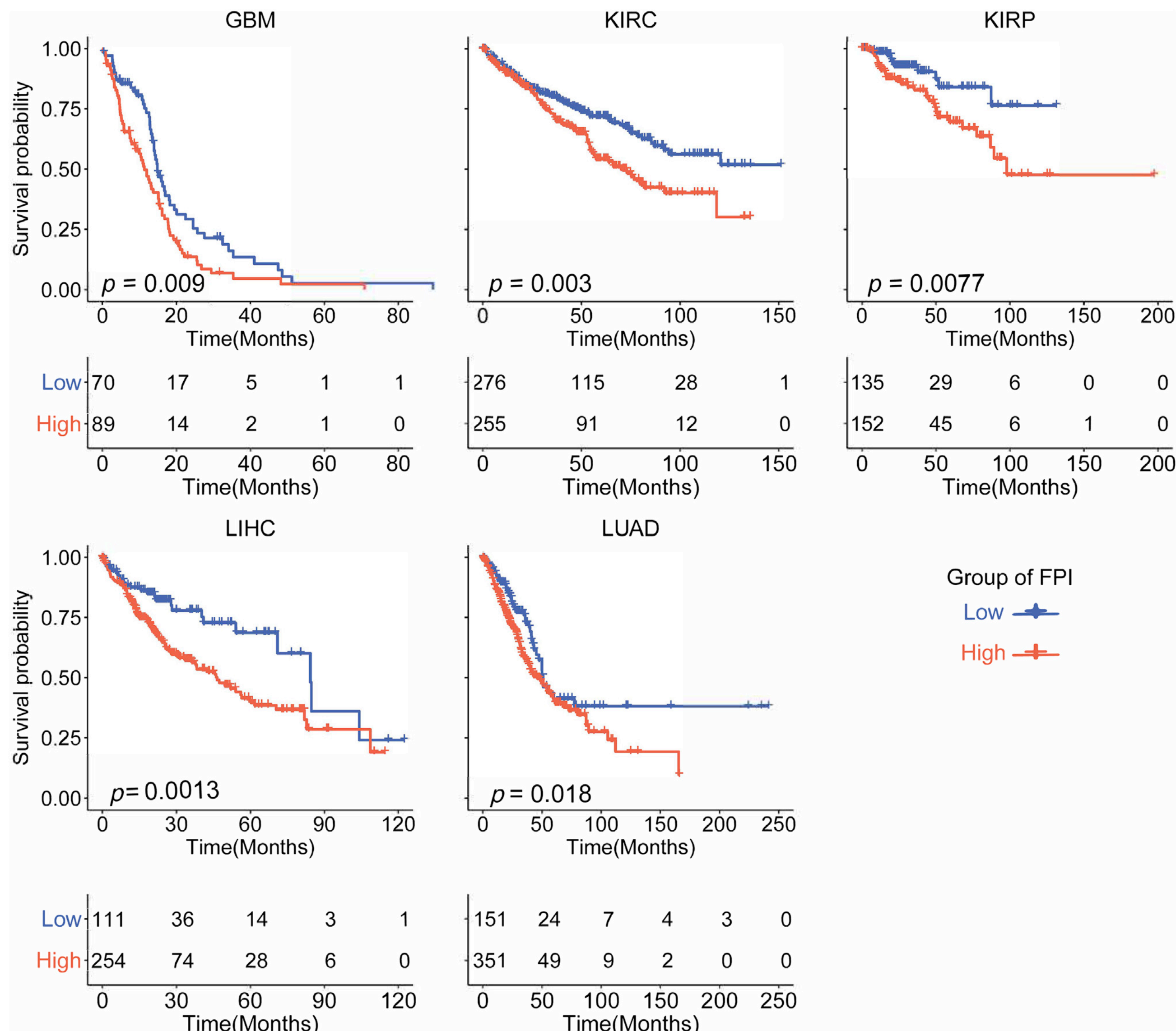

Figure 4. Kaplan-Meier Analysis of Overall Survival according to the FPI among Cancers

indicate that ferroptosis might play critical roles in cancer survival and that clinical factors have tumor-specific effects on FPI.

To further dissect the clinical relevance of ferroptosis in cancer, the roles of FRGs in cancer survival were analyzed. The survival analysis showed that all FRGs were associated with overall survival in at least six cancer types (Figure S3I), but the correlations were mixed since most FRGs can serve as a protective or a risk factor in different cancers. For example, patients with higher expression of *FANCD2* showed better survival in kidney cancer, LIHC, and LUAD but worse survival in READ, STAD, and BLCA (Figure S3I). However, high expression of *CARS* and *MT1G* showed consistently better survival among cancers including KICH, UCEC, PAAD, and HNSC (Figure S3I). Thus, the functional roles of FRGs in cancer survival should be further explored.

To study the potential clinical implications of ferroptosis, we examined the association between the gene expression of FRGs and 156 clinically actionable genes (CAGs), including 136 genes for targeted therapy and 20 genes for immunotherapy across cancer types (Mak et al., 2016; Van Allen et al., 2014). As an FRG,

CDKN1A regulates iron uptake and *GPX4* abundance (Stockwell et al., 2017) and is also a CAG targeted by anticancer drugs, such as the inorganic compound arsenic trioxide (Hassani et al., 2018). We found that all 136 CAGs and FRGs had significant co-expression relationships that were significantly different across cancers as shown in Figure S4A. The number of CAGs correlated with FRGs ranged from 45 in LUSC to 132 in THCA (Figure S4B). The FRG-CAG correlation pairs ranged from 69 in LUSC to 581 in THCA (Figure S4C). For example, *GPX4* was co-expressed with *MAP2K2* in 20 cancer types and showed a significantly positive correlation with *TNFRSF4*, which are targeted genes for immunotherapy. *ACSL4* is significantly correlated with 17 of 20 genes targeted for immunotherapy, suggesting that *ACSL4* has a potential effect on cancer immunotherapy (Figure S4D). Furthermore, besides co-expression, the protein-protein interactions among drug-targeted CAGs and FRGs were analyzed, and the results presented in Figure S4E showed that the interactions were obvious. For example, *EGFR*, the target of lapatinib, gefitinib, and afatinib, was positively associated with FRGs, including *DPP4* ($R = 0.15$) and *HSPA5* ($R = 0.31$), and negatively correlated with *FDFT1* ($R = -0.24$), whereas there were protein-protein interactions between EGFR and DPP4, HSPA5, and FDFT1 (Figure S4E). These results indicated that ferroptosis might be involved in drug effects by interacting with targeted clinically actionable genes. Taken together, our studies suggest that clinically actionable genes are closely related to FRGs, which highlights the significance of ferroptosis in cancer treatment, including both immunotherapy and targeted therapy.

To further understand the correlation between ferroptosis and drug sensitivity, the area under the percent viability curve (AUC) approach was employed to evaluate drug sensitivity (Basu et al., 2013) and calculate the correlation between FPI and drug sensitivity across cancer cell lines. Drugs associated with FPI were also tested for their correlation with FRG expression. We identified that FPI was significantly associated with sensitivity to 64 drugs, including 12 that were negatively correlated and 52 that were positively correlated (Figure S4F). To explore the effects of each FRG on drug sensitivity, we also analyzed the associations between the drug sensitivity of 64 cancer drugs and the expression of FRGs and found 521 significantly correlated pairs (Figure S4F). Among them, the expression of *FANCD2* was correlated with the AUC of 57 drugs, whereas no significant relation was observed for *CISD1* (Figure S4F). Furthermore, the associations classified the FRGs into two groups: One group included genes such as *FANCD2* and *ATP5G3*, which were positively associated with the AUC of docetaxel, trametinib, etc. (Figure S4F). The other group included *SLC7A11*, *SAT1*, and *HSPA5*, which were negatively associated with the AUC values (Figure S4F). Taken together, these results suggest that ferroptosis is correlated with the sensitivity of multiple drugs.

DISCUSSION

Ferroptosis is driven by damage of cell membranes caused by the loss of activity of GPX4 (Feng and Stockwell, 2018). Researchers identified that ferroptosis is closely related to tumorigenesis and plays an important role in cancer treatment (Shen et al., 2018; Yang et al., 2014). However, there is a lack of systematic studies on ferroptosis and its regulator genes across cancer types. In this study, we employed multi-omics data and clinical data across 20 cancer types from TCGA and revealed the global alterations of ferroptosis regulator genes at genetic, epigenetic, and transcriptional levels. We also used ssGSEA to process expression data to establish FPI to characterize ferroptosis and addressed which genetic and nongenetic factors (including drug and patient phenotype) were related with FPI. Different molecular types affected the ferroptosis in breast cancer and gastrointestinal cancer, which meant that the responses of different molecular subtypes to treatment may be related to ferroptosis. On the other hand, molecular subtypes need to be considered when ferroptosis is applied as a therapeutic strategy.

The mechanism by which ferroptosis regulates tumor cell growth and proliferation is still unclear, but the relationship we observed between FPI and hallmarks of cancer could improve the understanding the role of ferroptosis. The results of GSEA demonstrate that the level of ferroptosis is closely related to tumor-associated hallmarks in most cancers. Ferroptosis genes can play both oncogene and tumor suppressor roles in cancer (Kang et al., 2019), and the FPI acts as a protective or risk factor across cancer types. We also found that several common clinical factors affected ferroptosis, such as cigarette smoking, BMI, and tumor stage. As we know, cigarette smoking is a risk factor for esophageal cancer, lung cancer, and kidney cancer (Chow et al., 2010; Mao et al., 2011; Pesch et al., 2012). In our results, the number of cigarettes per day was positively correlated with the ferroptosis potential index in LUAD, which may be because the cigarette-induced oxidation reaction promoted lipid peroxidation (Barreiro et al., 2010; Guan et al., 2013; Louhelainen et al., 2008). FPI also varied between the sexes in several cancers, including LIHC, LUAD, LUSC, and STAD, and between different races in BRCA, BLCA, and ESCA, which implied that gender and race need to be

considered when using ferroptosis as a treatment strategy. We also noticed that better clinical outcomes or status in several cancer types also have lower FPI, which further confirmed the dual role of ferroptosis. Thus, a different strategy of regulating the ferroptosis of tumor cells may benefit patients and improve prognosis.

Furthermore, we showed that FRGs were co-expressed with most clinically actionable genes and interacted with genes modulated by drugs, suggesting that studying ferroptosis may improve the strategy for cancer therapy. We observed that the co-expression of FRGs and CAGs could be roughly divided into two groups and drugs that target clinical genes could have complex regulatory effects, which indicated that clinically actionable gene *MAP2K2* may play an important role in ferroptosis (Yang et al., 2014). To further explore drug sensitivity and ferroptosis, we observed that the FPI could characterize the sensitivity of many drugs, the AUC of many drugs was inversely associated with the FPI in cancer cell lines, which implied that regulating the ferroptosis of tumor cells may improve the therapeutic effect of cancer treatments. However, opposite effects were observed regarding the effects of drugs on ferroptosis. Thus, further detailed studies should be carried out to determine the functions and mechanisms of ferroptosis in different cancers. In the present study, we presented a systematical analysis of ferroptosis and its regulator genes across cancers. Most FRGs were aberrantly expressed in tumors among various cancer types, while frequent CNA and differential DNA methylation contributed greatly. We established the FPI to evaluate the ferroptosis level and found that the FPIs were higher in tumors than in the adjacent normal tissues in most cancers and were associated with clinical features, and cancer metastasis, recurrence, outcome, and drug sensitivity. Several well-known anti-cancer drugs were also reported to induce ferroptosis, such as sorafenib, which was used to treat renal cell carcinoma and hepatocellular carcinoma (Louandre et al., 2015; Yang et al., 2014). In addition, small molecule inducers based on the mechanism of system Xc- inhibition or GPX4 inhibition were considered as a therapeutic strategy for cancer (Yang et al., 2014). Thus, our findings highlighted the potential of ferroptosis-based cancer therapy.

Limitations of the Study

Since current omics data only provide RNA-level quantifications for FRGs, whereas the ferroptosis process relies on proteins, although we tried to infer the ferroptosis status precisely, there could be a variety of inaccuracies. Furthermore, the detailed molecular mechanisms for ferroptosis are still unclear, and currently, the identified FRGs and the genes used for modeling ferroptosis potential have various other functions; thus, the sensitivity and specificity of FPI might be limited. In addition, although the transcriptome datasets of cell lines treated with erastin, withaferin A, or ferrostatin indicated that the FPI was accurate, since the transcriptome datasets with well-characterized ferroptosis status were rare, the *bona fide* accuracy of the FPI still needs further evaluation. Thus, our study based on current knowledge might need further updates and improvements due to new discoveries.

Resource Availability

Lead Contact

Further information and requests for resources should be directed to and will be fulfilled by the Lead Contact, Ze-Xian Liu (liuzx@sysucc.org.cn).

Materials Availability

This study did not generate new unique reagents.

Data and Code Availability

GSVA (version: 1.30) is available at https://github.com/rcastelo/GSVA.

The TCGA cohort data: The mRNA expression data, copy number alteration thresholded data, masked copy number segmentation data, and DNA methylation 450K data were download from Firehose (http://gdac.broadinstitute.org). Mutation data, miRNA-seq data, and clinical data were downloaded from the Xena Browser (https://xenabrowser.net/datapages/). Tumor suppressor gene lists and oncogene lists were retrieved from Bailey et al. (2018). The information of microsatellite instability of TCGA tumor samples were retrieved from Liu, Y et al. (Liu et al., 2018).

Immune associated data: Immune cell and immunophenotype data were requested from The Cancer Immunome Atlas (https://tcia.at/home) (Charoentong et al., 2017). Dysfunction and exclusion scores were retrieved from TIDE (http://tide.dfci.harvard.edu/) (Fu et al., 2020).

Protein-protein interaction data was download from the Human Protein Reference Database (http://www.hprd.org/) and BioGRID (https://thebiogrid.org).

METHODS

All methods can be found in the accompanying Transparent Methods supplemental file.

SUPPLEMENTAL INFORMATION

Supplemental Information can be found online at https://doi.org/10.1016/j.isci.2020.101302.

ACKNOWLEDGMENTS

This work was supported by grants from National Key R&D Program of China (2018YFC1313300 to RH.X.), Program for Guangdong Introducing Innovative and Entrepreneurial Teams (2017ZT07S096 to ZX.L.), Tip-top Scientific and Technical Innovative Youth Talents of Guangdong Special Support Program (2019TQ05Y351 to ZX.L.), CAMS Innovation Fund for Medical Sciences (2019-I2M-5-036 to RH.X.), Natural Science Foundation of Guangdong Province (2017A030313485 to RH.X., 2019A1515010634 to ZX.L.), Fundamental Research Funds for the Central Universities (SYSU: 19ykpy184 to Q.Z.), Natural Science Foundation of China (81802438 to Q.Z.), and Science and Technology Program of Guangdong (2019B020227002 to RH.X.).

AUTHOR CONTRIBUTIONS

ZX.L. and RH.X. designed and supervised the experiments. Z.L., Q.Z., ZX.Z., and SQ.Y. performed the data analysis with contributions from K.Y., Q.Z., X.Z., H.S., HQ.J., H.C., and F.W. ZX.L. and Z.L. wrote the manuscript with contributions of all authors. All authors reviewed the manuscript.

DECLARATION OF INTERESTS

The authors declare that they have no competing interests.

Received: February 19, 2020
Revised: April 9, 2020
Accepted: June 17, 2020
Published: July 24, 2020

REFERENCES

Bailey, M.H., Tokheim, C., Porta-Pardo, E., Sengupta, S., Bertrand, D., Weerasinghe, A., Colaprico, A., Wendl, M.C., Kim, J., Reardon, B., et al. (2018). Comprehensive characterization of cancer driver genes and mutations. Cell *173*, 371–385.e18.

Barreiro, E., Peinado, V.I., Galdiz, J.B., Ferrer, E., Marin-Corral, J., Sanchez, F., Gea, J., Barbera, J.A., and Project, E.i.C. (2010). Cigarette smoke-induced oxidative stress: a role in chronic obstructive pulmonary disease skeletal muscle dysfunction. Am. J. Respir. Crit. Care Med. *182*, 477–488.

Basu, A., Bodycombe, N.E., Cheah, J.H., Price, E.V., Liu, K., Schaefer, G.I., Ebright, R.Y., Stewart, M.L., Ito, D., Wang, S., et al. (2013). An interactive resource to identify cancer genetic and lineage dependencies targeted by small molecules. Cell *154*, 1151–1161.

Canisius, S., Martens, J.W., and Wessels, L.F. (2016). A novel independence test for somatic alterations in cancer shows that biology drives mutual exclusivity but chance explains most co-occurrence. Genome Biol. *17*, 261.

Charoentong, P., Finotello, F., Angelova, M., Mayer, C., Efremova, M., Rieder, D., Hackl, H., and Trajanoski, Z. (2017). Pan-cancer immunogenomic analyses reveal genotype-immunophenotype relationships and predictors of response to checkpoint blockade. Cell Rep. *18*, 248–262.

Chow, W.H., Dong, L.M., and Devesa, S.S. (2010). Epidemiology and risk factors for kidney cancer. Nat. Rev. Urol. *7*, 245–257.

Dixon, S.J., Lemberg, K.M., Lamprecht, M.R., Skouta, R., Zaitsev, E.M., Gleason, C.E., Patel, D.N., Bauer, A.J., Cantley, A.M., Yang, W.S., et al. (2012). Ferroptosis: an iron-dependent form of nonapoptotic cell death. Cell *149*, 1060–1072.

Dixon, S.J., Winter, G.E., Musavi, L.S., Lee, E.D., Snijder, B., Rebsamen, M., Superti-Furga, G., and Stockwell, B.R. (2015). Human haploid cell genetics reveals roles for lipid metabolism genes in nonapoptotic cell death. ACS Chem. Biol. *10*, 1604–1609.

Doll, S., Proneth, B., Tyurina, Y.Y., Panzilius, E., Kobayashi, S., Ingold, I., Irmler, M., Beckers, J., Aichler, M., Walch, A., et al. (2017). ACSL4 dictates ferroptosis sensitivity by shaping cellular lipid composition. Nat. Chem. Biol. *13*, 91–98.

Eling, N., Reuter, L., Hazin, J., Hamacher-Brady, A., and Brady, N.R. (2015). Identification of artesunate as a specific activator of ferroptosis in pancreatic cancer cells. Oncoscience *2*, 517–532.

Feng, H., and Stockwell, B.R. (2018). Unsolved mysteries: how does lipid peroxidation cause ferroptosis? PLoS Biol. *16*, e2006203.

Friedmann Angeli, J.P., Schneider, M., Proneth, B., Tyurina, Y.Y., Tyurin, V.A., Hammond, V.J., Herbach, N., Aichler, M., Walch, A., Eggenhofer, E., et al. (2014). Inactivation of the ferroptosis regulator Gpx4 triggers acute renal failure in mice. Nat. Cell Biol. *16*, 1180–1191.

Fu, J., Li, K., Zhang, W., Wan, C., Zhang, J., Jiang, P., and Liu, X.S. (2020). Large-scale public data reuse to model immunotherapy response and resistance. Genome Med. *12*, 21.

Guan, S.P., Tee, W., Ng, D.S., Chan, T.K., Peh, H.Y., Ho, W.E., Cheng, C., Mak, J.C., and Wong, W.S. (2013). Andrographolide protects against cigarette smoke-induced oxidative lung injury via

augmentation of Nrf2 activity. Br. J. Pharmacol. *168*, 1707–1718.

Hassani, S., Khaleghian, A., Ahmadian, S., Alizadeh, S., Alimoghaddam, K., Ghavamzadeh, A., and Ghaffari, S.H. (2018). Redistribution of cell cycle by arsenic trioxide is associated with demethylation and expression changes of cell cycle related genes in acute promyelocytic leukemia cell line (NB4). Ann. Hematol. *97*, 83–93.

Hassannia, B., Wiernicki, B., Ingold, I., Qu, F., Van Herck, S., Tyurina, Y.Y., Bayir, H., Abhari, B.A., Angeli, J.P.F., Choi, S.M., et al. (2018). Nano-targeted induction of dual ferroptotic mechanisms eradicates high-risk neuroblastoma. J. Clin. Invest. *128*, 3341–3355.

Inder, T., Mocatta, T., Darlow, B., Spencer, C., Volpe, J.J., and Winterbourn, C. (2002). Elevated free radical products in the cerebrospinal fluid of VLBW infants with cerebral white matter injury. Pediatr. Res. *52*, 213–218.

Kang, R., Kroemer, G., and Tang, D. (2019). The tumor suppressor protein p53 and the ferroptosis network. Free Radic. Biol. Med. *133*, 162–168.

Kettner, N.M., Voicu, H., Finegold, M.J., Coarfa, C., Sreekumar, A., Putluri, N., Katchy, C.A., Lee, C., Moore, D.D., and Fu, L. (2016). Circadian homeostasis of liver metabolism suppresses hepatocarcinogenesis. Cancer Cell *30*, 909–924.

Li, J.H., Liu, S., Zhou, H., Qu, L.H., and Yang, J.H. (2014). starBase v2.0: decoding miRNA-ceRNA, miRNA-ncRNA and protein-RNA interaction networks from large-scale CLIP-Seq data. Nucleic Acids Res. *42*, D92–D97.

Linkermann, A., Skouta, R., Himmerkus, N., Mulay, S.R., Dewitz, C., De Zen, F., Prokai, A., Zuchtriegel, G., Krombach, F., Welz, P.S., et al. (2014). Synchronized renal tubular cell death involves ferroptosis. Proc. Natl. Acad. Sci. U S A *111*, 16836–16841.

Liu, Y., Sethi, N.S., Hinoue, T., Schneider, B.G., Cherniack, A.D., Sanchez-Vega, F., Seoane, J.A., Farshidfar, F., Bowlby, R., Islam, M., et al. (2018). Comparative molecular analysis of gastrointestinal adenocarcinomas. Cancer Cell *33*, 721–735.e8.

Louandre, C., Ezzoukhry, Z., Godin, C., Barbare, J.C., Maziere, J.C., Chauffert, B., and Galmiche, A. (2013). Iron-dependent cell death of hepatocellular carcinoma cells exposed to sorafenib. Int. J. Cancer *133*, 1732–1742.

Louandre, C., Marcq, I., Bouhlal, H., Lachaier, E., Godin, C., Saidak, Z., Francois, C., Chatelain, D., Debuysscher, V., Barbare, J.C., et al. (2015). The retinoblastoma (Rb) protein regulates ferroptosis induced by sorafenib in human hepatocellular carcinoma cells. Cancer Lett. *356*, 971–977.

Louhelainen, N., Myllarniemi, M., Rahman, I., and Kinnula, V.L. (2008). Airway biomarkers of the oxidant burden in asthma and chronic obstructive pulmonary disease: current and future perspectives. Int. J. Chron. Obstruct. Pulmon. Dis. *3*, 585–603.

Lu, B., Chen, X.B., Ying, M.D., He, Q.J., Cao, J., and Yang, B. (2017). The role of ferroptosis in cancer development and treatment response. Front. Pharmacol. *8*, 992.

Macfarlane, L.A., and Murphy, P.R. (2010). MicroRNA: biogenesis, function and role in cancer. Curr. Genomics *11*, 537–561.

Mak, M.P., Tong, P., Diao, L., Cardnell, R.J., Gibbons, D.L., William, W.N., Skoulidis, F., Parra, E.R., Rodriguez-Canales, J., Wistuba, I.I., et al. (2016). A patient-derived, pan-cancer EMT signature identifies global molecular alterations and immune target enrichment following epithelial-to-mesenchymal transition. Clin. Cancer Res. *22*, 609–620.

Mao, W.M., Zheng, W.H., and Ling, Z.Q. (2011). Epidemiologic risk factors for esophageal cancer development. Asian Pac. J. Cancer Prev. *12*, 2461–2466.

Masur, K., Schwartz, F., Entschladen, F., Niggemann, B., and Zaenker, K.S. (2006). DPPIV inhibitors extend GLP-2 mediated tumour promoting effects on intestinal cancer cells. Regul. Pept. *137*, 147–155.

Matsushita, M., Freigang, S., Schneider, C., Conrad, M., Bornkamm, G.W., and Kopf, M. (2015). T cell lipid peroxidation induces ferroptosis and prevents immunity to infection. J. Exp. Med. *212*, 555–568.

Pesch, B., Kendzia, B., Gustavsson, P., Jockel, K.H., Johnen, G., Pohlabeln, H., Olsson, A., Ahrens, W., Gross, I.M., Bruske, I., et al. (2012). Cigarette smoking and lung cancer–relative risk estimates for the major histological types from a pooled analysis of case-control studies. Int. J. Cancer *131*, 1210–1219.

Pro, B., and Dang, N.H. (2004). CD26/dipeptidyl peptidase IV and its role in cancer. Histol. Histopathol. *19*, 1345–1351.

Shen, H., and Laird, P.W. (2013). Interplay between the cancer genome and epigenome. Cell *153*, 38–55.

Shen, Z., Song, J., Yung, B.C., Zhou, Z., Wu, A., and Chen, X. (2018). Emerging strategies of cancer therapy based on ferroptosis. Adv. Mater. *30*, e1704007.

Skouta, R., Dixon, S.J., Wang, J., Dunn, D.E., Orman, M., Shimada, K., Rosenberg, P.A., Lo, D.C., Weinberg, J.M., Linkermann, A., et al. (2014). Ferrostatins inhibit oxidative lipid damage and cell death in diverse disease models. J. Am. Chem. Soc. *136*, 4551–4556.

Stockwell, B.R., Friedmann Angeli, J.P., Bayir, H., Bush, A.I., Conrad, M., Dixon, S.J., Fulda, S., Gascon, S., Hatzios, S.K., Kagan, V.E., et al. (2017). Ferroptosis: a regulated cell death nexus linking metabolism, redox biology, and disease. Cell *171*, 273–285.

Sun, X., Niu, X., Chen, R., He, W., Chen, D., Kang, R., and Tang, D. (2016a). Metallothionein-1G facilitates sorafenib resistance through inhibition of ferroptosis. Hepatology *64*, 488–500.

Sun, X., Ou, Z., Chen, R., Niu, X., Chen, D., Kang, R., and Tang, D. (2016b). Activation of the p62-Keap1-NRF2 pathway protects against ferroptosis in hepatocellular carcinoma cells. Hepatology *63*, 173–184.

Tsoi, J., Robert, L., Paraiso, K., Galvan, C., Sheu, K.M., Lay, J., Wong, D.J.L., Atefi, M., Shirazi, R., Wang, X., et al. (2018). Multi-stage differentiation defines melanoma subtypes with differential vulnerability to drug-induced iron-dependent oxidative stress. Cancer Cell *33*, 890–904.e5.

Van Allen, E.M., Wagle, N., Stojanov, P., Perrin, D.L., Cibulskis, K., Marlow, S., Jane-Valbuena, J., Friedrich, D.C., Kryukov, G., Carter, S.L., et al. (2014). Whole-exome sequencing and clinical interpretation of formalin-fixed, paraffin-embedded tumor samples to guide precision cancer medicine. Nat. Med. *20*, 682–688.

Wang, W., Green, M., Choi, J.E., Gijón, M., Kennedy, P.D., Johnson, J.K., Liao, P., Lang, X., Kryczek, I., Sell, A., et al. (2019). CD8+ T cells regulate tumour ferroptosis during cancer immunotherapy. Nature *569*, 270–274.

Wesley, U.V., McGroarty, M., and Homoyouni, A. (2005). Dipeptidyl peptidase inhibits malignant phenotype of prostate cancer cells by blocking basic fibroblast growth factor signaling pathway. Cancer Res. *65*, 1325–1334.

Xie, Y., Zhu, S., Song, X., Sun, X., Fan, Y., Liu, J., Zhong, M., Yuan, H., Zhang, L., Billiar, T.R., et al. (2017). The tumor suppressor p53 limits ferroptosis by blocking DPP4 activity. Cell Rep. *20*, 1692–1704.

Yang, W.S., SriRamaratnam, R., Welsch, M.E., Shimada, K., Skouta, R., Viswanathan, V.S., Cheah, J.H., Clemons, P.A., Shamji, A.F., Clish, C.B., et al. (2014). Regulation of ferroptotic cancer cell death by GPX4. Cell *156*, 317–331.

Yang, W.S., and Stockwell, B.R. (2016). Ferroptosis: death by lipid peroxidation. Trends Cell Biol. *26*, 165–176.

Yu, H., Guo, P., Xie, X., Wang, Y., and Chen, G. (2017). Ferroptosis, a new form of cell death, and its relationships with tumourous diseases. J. Cell. Mol. Med. *21*, 648–657.

Zhang, X., Du, L., Qiao, Y., Zhang, X., Zheng, W., Wu, Q., Chen, Y., Zhu, G., Liu, Y., Bian, Z., et al. (2019). Ferroptosis is governed by differential regulation of transcription in liver cancer. Redox Biol. *24*, 101211.

iScience, Volume *23*

Supplemental Information

Systematic Analysis of the Aberrances and Functional Implications of Ferroptosis in Cancer

Zekun Liu, Qi Zhao, Zhi-Xiang Zuo, Shu-Qiang Yuan, Kai Yu, Qingfeng Zhang, Xiaolong Zhang, Hui Sheng, Huai-Qiang Ju, Han Cheng, Feng Wang, Rui-Hua Xu, and Ze-Xian Liu

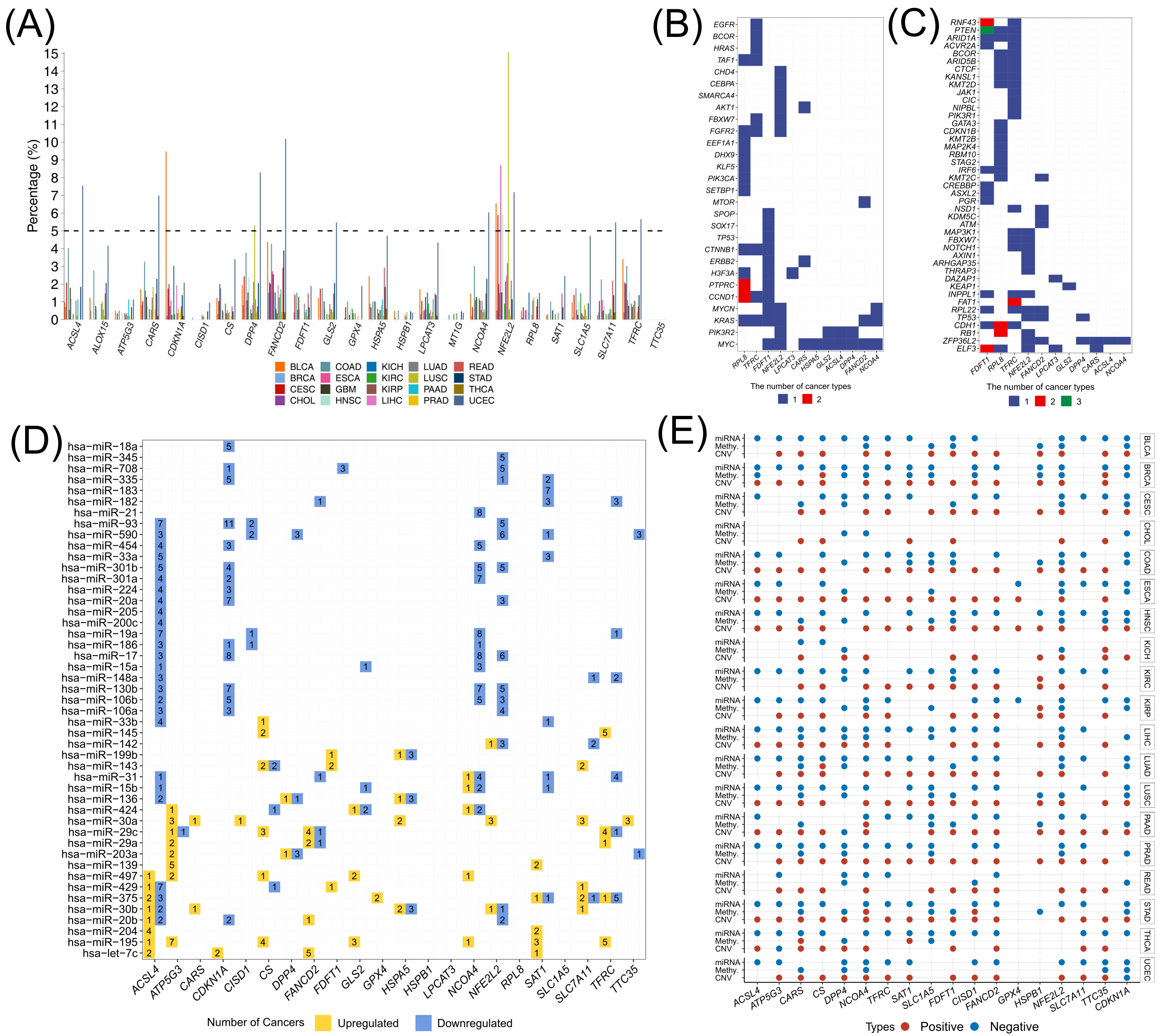

Figure S1. Molecular alterations of FRGs. Related to Figure 1.

The mutation frequencies (A), mutual exclusivity of FRGs and oncogenes (B) /tumor suppressor genes (C) among cancers. (D) The differential expressed FRGs-related miRNAs. The correlation between FRG expression and somatic copy number alternation, DNA methylation and miRNA expressions.

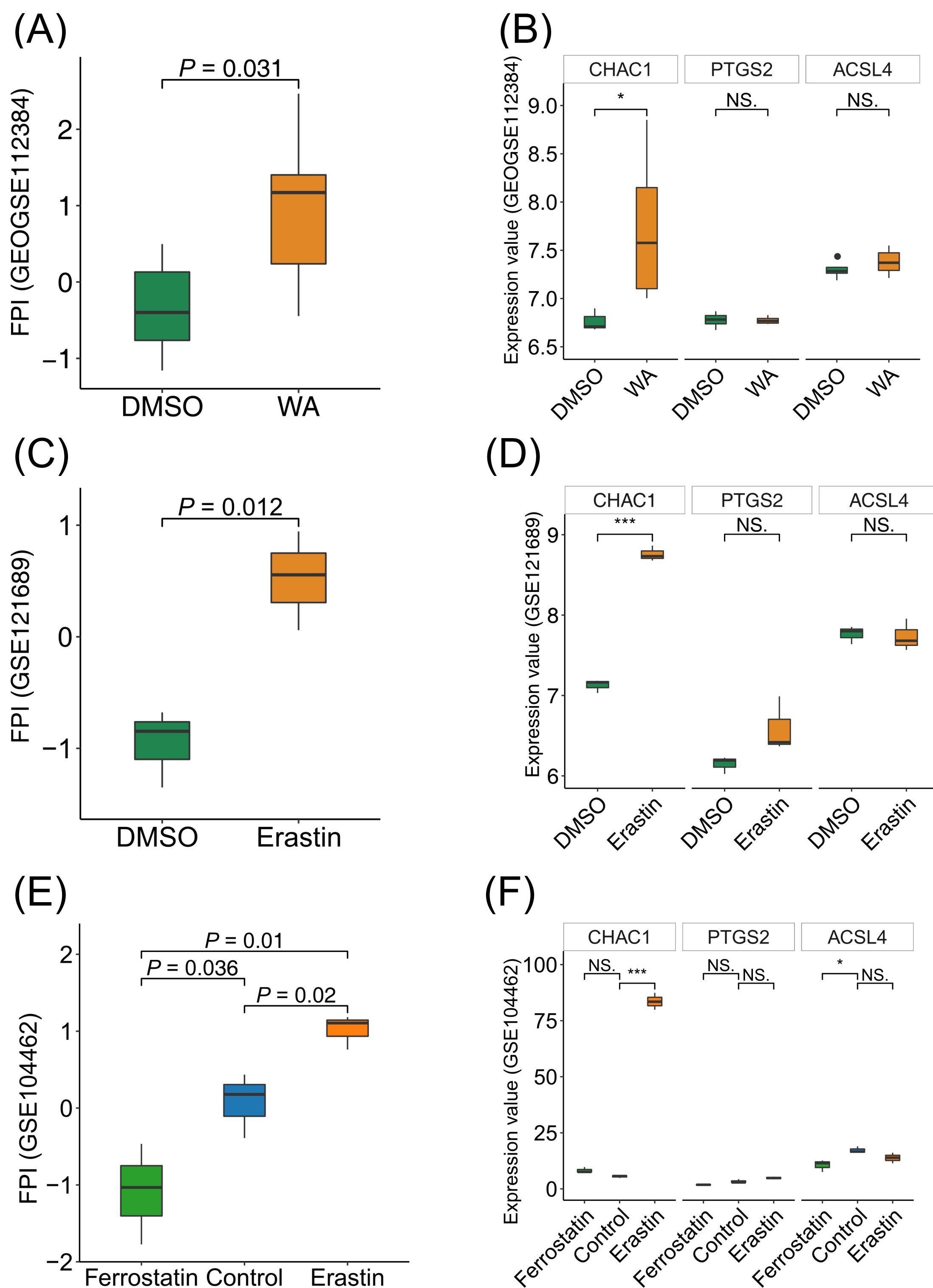

Figure S2. Established the FPI in cell lines and examined the performance of the FPI. Related to Figure 2.

The boxes showed the FPI between withaferin A (WA), erastin or ferrostatin and the control (A, D, G). The boxes showed the comparison of three genes between stimulators and control in neuroblastoma cells (B), clear cell carcinoma cells (E) and liver cancer cells (H). The correlation between the expression of *CHAC1* and the FPI in neuroblastoma cells (C), clear cell carcinoma cells (F) and liver cancer cells (I). The boxes in A-F mean the median values ± 1 quartile, their whiskers extending from the median to the smallest or biggest value which is 1.5 × IQR from the boundary of boxes. NS. indicates not significant (*p* value > 0.05), * *p* value < 0.05; ** *p* value < 0.01; *** *p* value < 0.001.

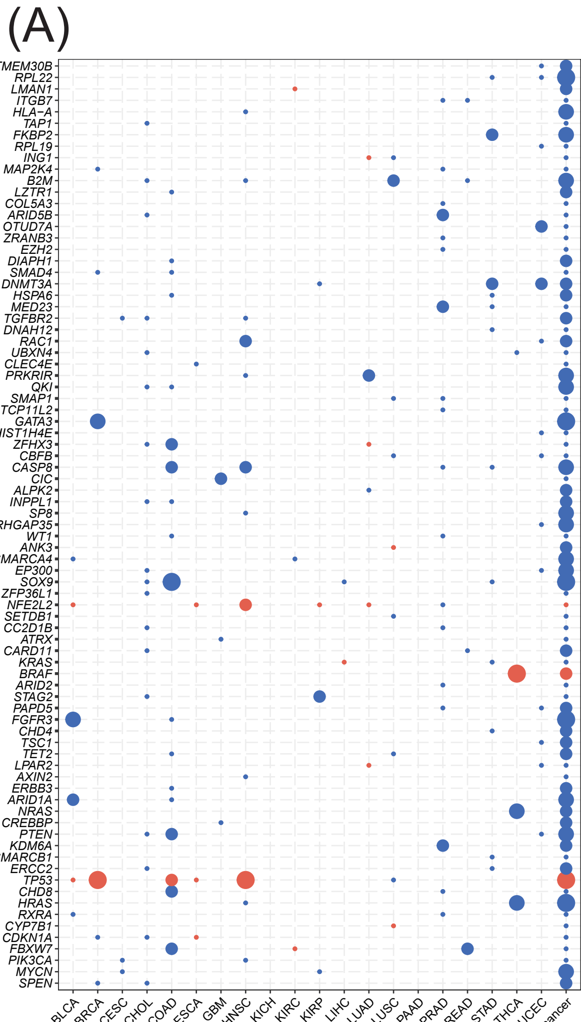
(A)
TMEM30B
RPL22
LMAN1
ITGB7
HLA−A
TAP1
FKBP2
RPL19
ING1
MAP2K4
B2M
LZTR1
COL5A3
ARID5B
OTUD7A
ZRANB3
EZH2
DIAPH1
SMAD4
DNMT3A
HSPA6
MED23
TGFBR2
DNAH12
RAC1
UBXN4
CLEC4E
PRKRIR
QKI
SMAP1
TCP11L2
GATA3
HIST1H4E
ZFHX3
CBFB
CASP8
CIC
ALPK2
INPPL1
SP8
ARHGAP35
WT1
ANK3
SMARCA4
EP300
SOX9
ZFP36L1
NFE2L2
SETDB1
CC2D1B
ATRX
CARD11
KRAS
BRAF
ARID2
STAG2
PAPD5
FGFR3
CHD4
TSC1
TET2
LPAR2
AXIN2
ERBB3
ARID1A
NRAS
CREBBP
PTEN
KDM6A
SMARCB1
ERCC2
TP53
CHD8
HRAS
RXRA
CYP7B1
CDKN1A
FBXW7
PIK3CA
MYCN
SPEN
BLCA
BRCA
CESC
CHOL
COAD
ESCA
GBM
HNSC
KICH
KIRC
KIRP
LIHC
LUAD
LUSC
PAAD
PRAD
READ
STAD
THCA
UCEC
Pan−cancer
Type negative positive
P value/FDR • < 0.05 • < 0.01 • < 0.001 • < 0.0001

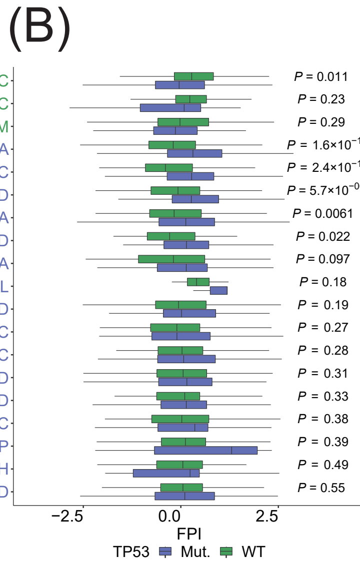
(B)
LUSC P = 0.011
KIRC P = 0.23
GBM P = 0.29
BRCA P = 1.6×10−17
HNSC P = 2.4×10−10
COAD P = 5.7×10−06
BLCA P = 0.0061
READ P = 0.022
ESCA P = 0.097
CHOL P = 0.18
PRAD P = 0.19
UCEC P = 0.27
LIHC P = 0.28
LUAD P = 0.31
PAAD P = 0.33
CESC P = 0.38
KIRP P = 0.39
KICH P = 0.49
STAD P = 0.55
−2.5
0.0
2.5
FPI
TP53 Mut. WT

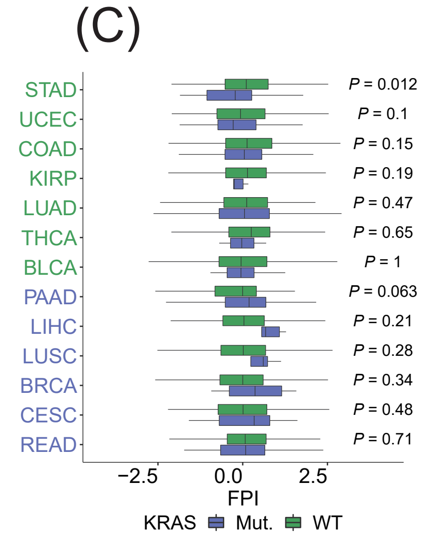
(C)
STAD P = 0.012
UCEC P = 0.1
COAD P = 0.15
KIRP P = 0.19
LUAD P = 0.47
THCA P = 0.65
BLCA P = 1
PAAD P = 0.063
LIHC P = 0.21
LUSC P = 0.28
BRCA P = 0.34
CESC P = 0.48
READ P = 0.71
−2.5
0.0
2.5
FPI
KRAS Mut. WT

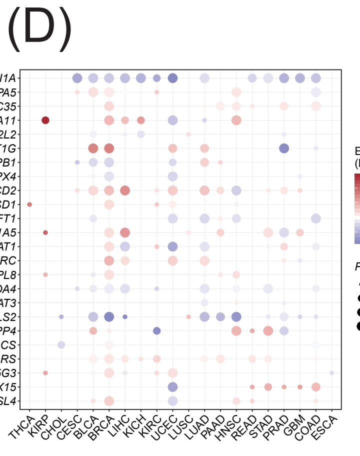
(D)
CDKN1A
HSPA5
TTC35
SLC7A11
NFE2L2
MT1G
HSPB1
GPX4
FANCD2
CISD1
FDFT1
SLC1A5
SAT1
TFRC
RPL8
NCOA4
LPCAT3
GLS2
DPP4
CS
CARS
ATP5G3
ALOX15
ACSL4
THCA
KIRP
CHOL
CESC
BLCA
BRCA
LIHC
KICH
KIRC
UCEC
LUSC
LUAD
PAAD
HNSC
READ
STAD
PRAD
GBM
COAD
ESCA
Exp. (Mut./Wild)
2
1
0
−1
P value
< 0.05
< 0.01
< 0.001
< 0.0001

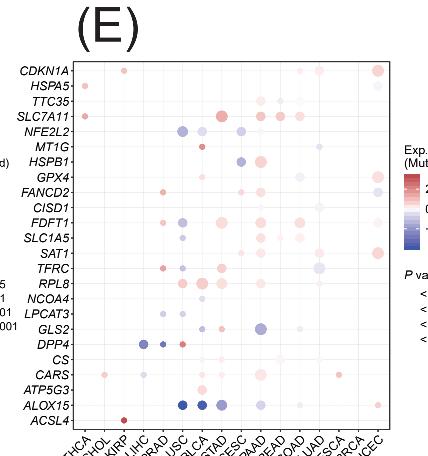
(E)
CDKN1A
HSPA5
TTC35
SLC7A11
NFE2L2
MT1G
HSPB1
GPX4
FANCD2
CISD1
FDFT1
SLC1A5
SAT1
TFRC
RPL8
NCOA4
LPCAT3
GLS2
DPP4
CS
CARS
ATP5G3
ALOX15
ACSL4
THCA
CHOL
KIRP
LIHC
PRAD
LUSC
BLCA
STAD
CESC
PAAD
READ
COAD
LUAD
ESCA
BRCA
UCEC
Exp. (Mut./Wild)
2
0
−2
P value
< 0.05
< 0.01
< 0.001
< 0.0001

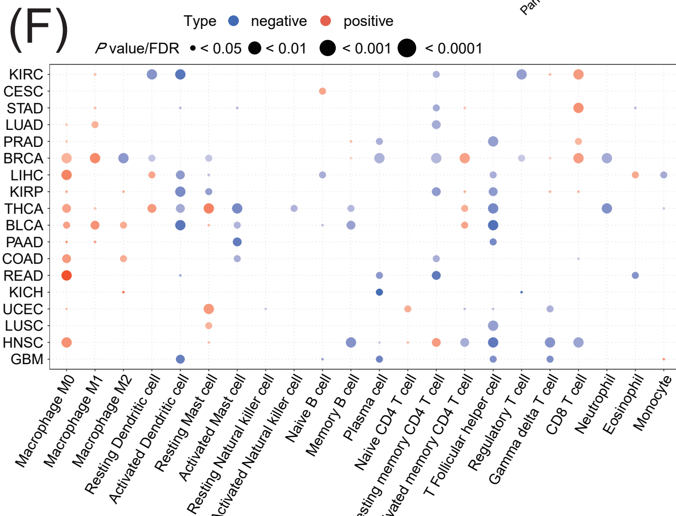
(F)
KIRC
CESC
STAD
LUAD
PRAD
BRCA
LIHC
KIRP
THCA
BLCA
PAAD
COAD
READ
KICH
UCEC
LUSC
HNSC
GBM
Macrophage M0
Macrophage M1
Macrophage M2
Resting Dendritic cell
Activated Dendritic cell
Resting Mast cell
Activated Mast cell
Resting Natural killer cell
Activated Natural killer cell
Naive B cell
Memory B cell
Plasma cell
Naive CD4 T cell
Resting memory CD4 T cell
Activated memory CD4 T cell
T Follicular helper cell
Regulatory T cell
Gamma delta T cell
CD8 T cell
Neutrophil
Eosinophil
Monocyte
Correlation
0.3
0.2
0.1
0.0
−0.1
−0.2
−0.3
P value
< 0.05
< 0.01
< 0.001
< 0.0001

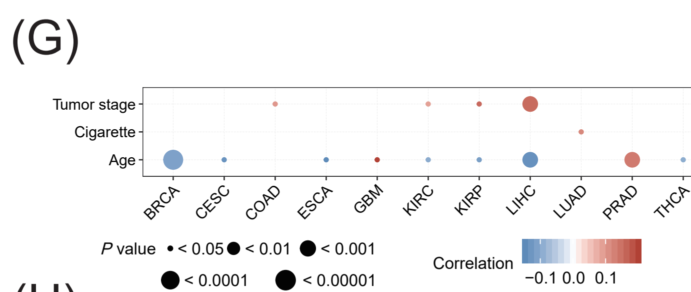
(G)
Tumor stage
Cigarette
Age
BRCA
CESC
COAD
ESCA
GBM
KIRC
KIRP
LIHC
LUAD
PRAD
THCA
P value • < 0.05 • < 0.01 • < 0.001 • < 0.0001 • < 0.00001
Correlation
−0.1 0.0 0.1

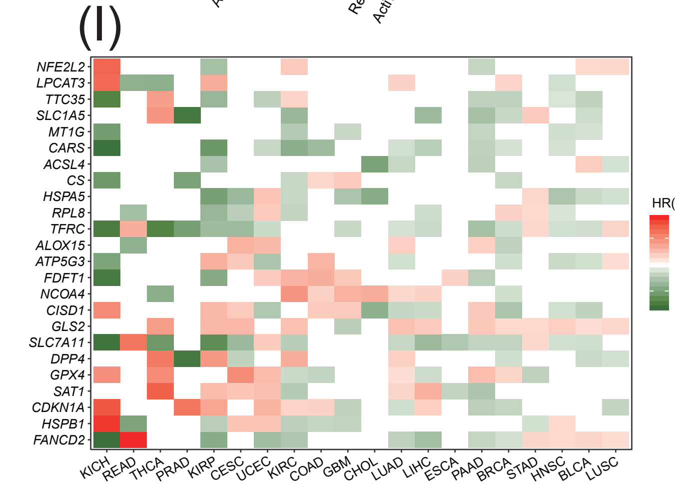
(I)
NFE2L2
LPCAT3
TTC35
SLC1A5
MT1G
CARS
ACSL4
CS
HSPA5
RPL8
TFRC
ALOX15
ATP5G3
FDFT1
NCOA4
CISD1
GLS2
SLC7A11
DPP4
GPX4
SAT1
CDKN1A
HSPB1
FANCD2
KICH
READ
THCA
PRAD
KIRP
CESC
UCEC
KIRC
COAD
GBM
CHOL
LUAD
LIHC
ESCA
PAAD
BRCA
STAD
HNSC
BLCA
LUSC
HR(log2)
2
0
−2

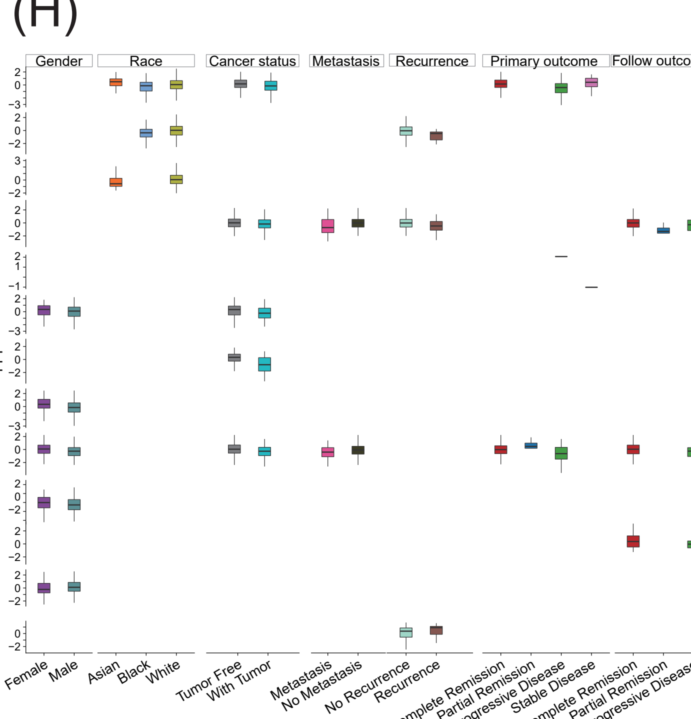
(H)
Gender
Race
Cancer status
Metastasis
Recurrence
Primary outcome
Follow outcome
FPI
BLCA
BRCA
ESCA
HNSC
KICH
KIRC
KIRP
LIHC
LUAD
LUSC
PAAD
STAD
THCA
Female
Male
Asian
Black
White
Tumor Free
With Tumor
Metastasis
No Metastasis
No Recurrence
Recurrence
Complete Remission
Partial Remission
Progressive Disease
Stable Disease
Complete Remission
Partial Remission
Progressive Disease

Figure S3. The relationship between other factors and the FPI or expression of FRGs. Related to Figure 2, Figure 3, and Figure 4.

The implication of the mutation status of driver genes on the FPI (A). The FPI between mutant and wild type tumors for *TP53* (B) and *KRAS* (C). The differential expression of FRGs between mutant and wild type tumors for *TP53* (D) and *KRAS* (E). The correlation between ferroptosis and immune cells (F) and clinical characteristics (G-H). The overall prognostic abilities of FRGs (I). The boxes in B, C, and H mean the median values $\pm$ 1 quartile, their whiskers extending from the median to the smallest or biggest value which is 1.5 $\times$ IQR from the boundary of boxes.

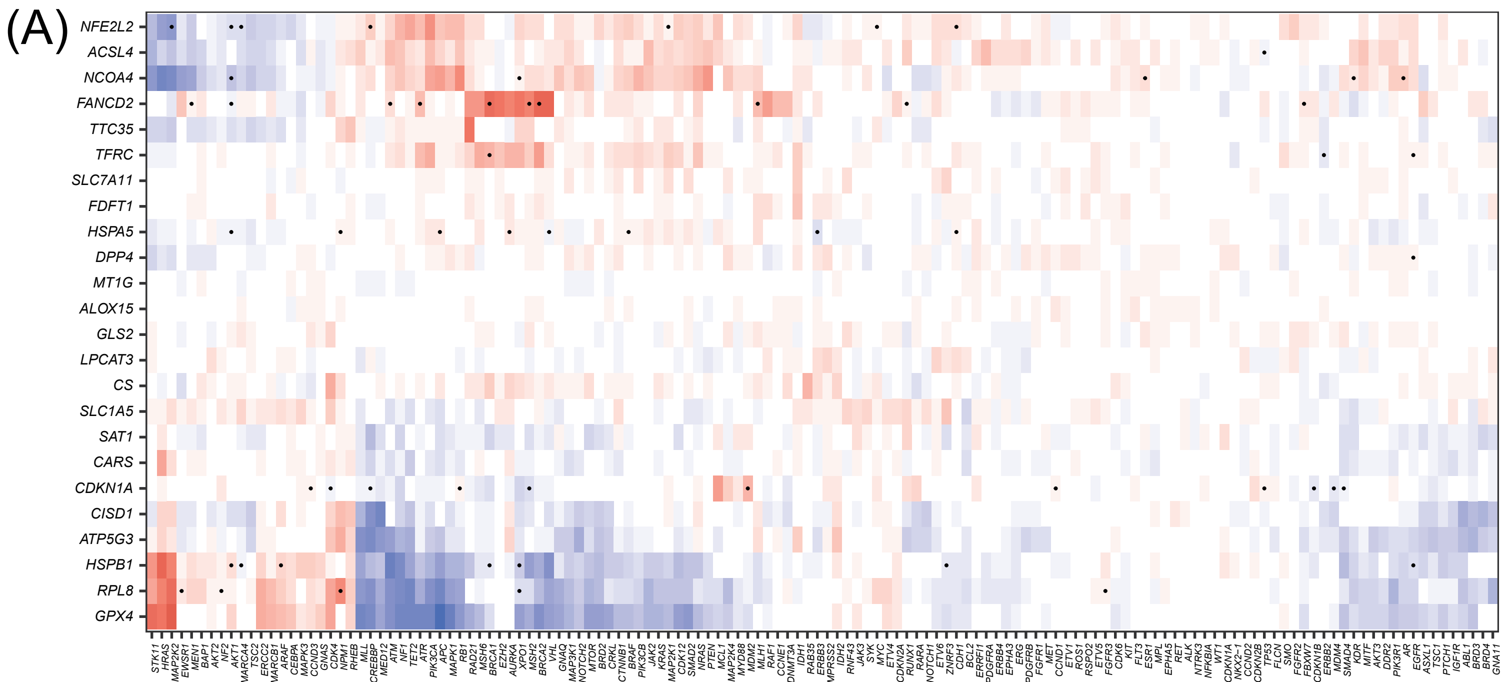
(A)
NFE2L2
ACSL4
NCOA4
FANCD2
TTC35
TFRC
SLC7A11
FDFT1
HSPA5
DPP4
MT1G
ALOX15
GLS2
LPCAT3
CS
SLC1A5
SAT1
CARS
CDKN1A
CISD1
ATP5G3
HSPB1
RPL8
GPX4
The number of cancer types
−10
0
10
20

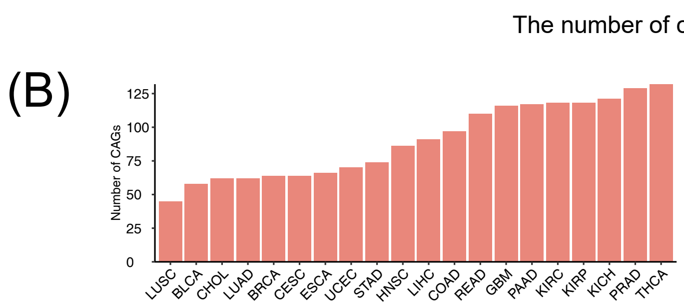
(B)
Number of CAGs
0
25
50
75
100
125
LUSC
BLCA
CHOL
LUAD
BRCA
CESC
ESCA
UCEC
STAD
HNSC
LIHC
COAD
READ
GBM
PAAD
KIRC
KIRP
KICH
PRAD
THCA

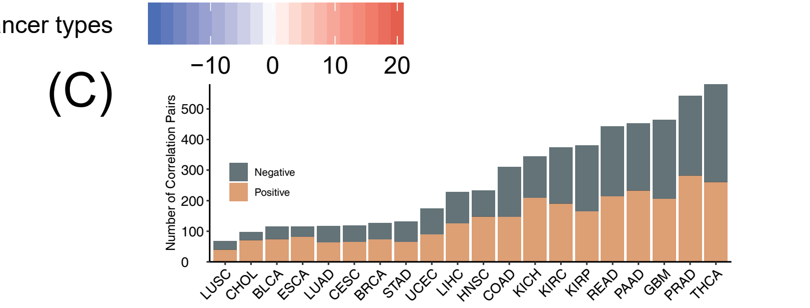
(C)
Number of Correlation Pairs
0
100
200
300
400
500
Negative
Positive
LUSC
CHOL
BLCA
ESCA
LUAD
CESC
BRCA
STAD
UCEC
LIHC
HNSC
COAD
KICH
KIRC
KIRP
READ
PAAD
GBM
PRAD
THCA

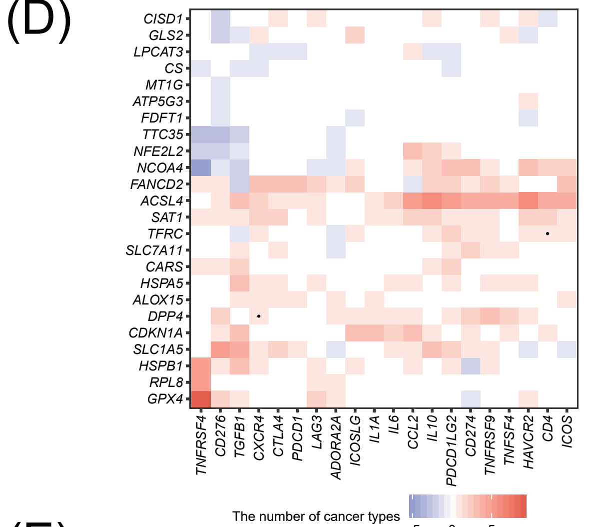
(D)
CISD1
GLS2
LPCAT3
CS
MT1G
ATP5G3
FDFT1
TTC35
NFE2L2
NCOA4
FANCD2
ACSL4
SAT1
TFRC
SLC7A11
CARS
HSPA5
ALOX15
DPP4
CDKN1A
SLC1A5
HSPB1
RPL8
GPX4
TNFRSF4
CD276
TGFB1
CXCR4
CTLA4
PDCD1
LAG3
ADORA2A
ICOSLG
IL1A
IL6
CCL2
IL10
PDCD1LG2
CD274
TNFRSF9
TNFSF4
HAVCR2
CD4
ICOS
The number of cancer types
−5
0
5

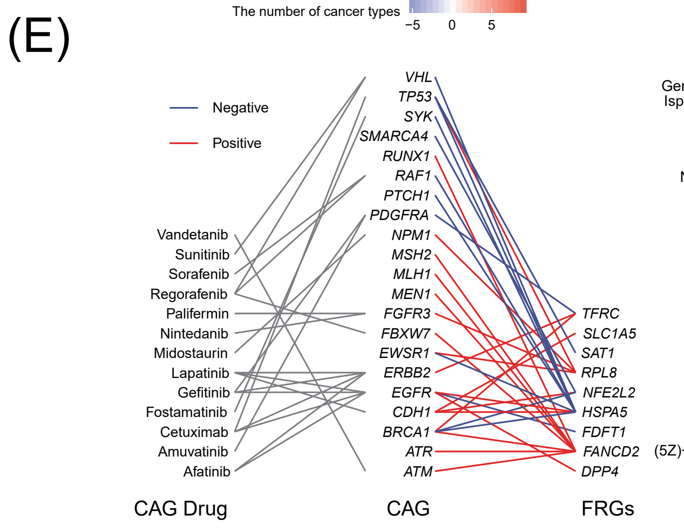
(E)
Negative
Positive
Vandetanib
Sunitinib
Sorafenib
Regorafenib
Palifermin
Nintedanib
Midostaurin
Lapatinib
Gefitinib
Fostamatinib
Cetuximab
Amuvatinib
Afatinib
VHL
TP53
SYK
SMARCA4
RUNX1
RAF1
PTCH1
PDGFRA
NPM1
MSH2
MLH1
MEN1
FGFR3
FBXW7
EWSR1
ERBB2
EGFR
CDH1
BRCA1
ATR
ATM
TFRC
SLC1A5
SAT1
RPL8
NFE2L2
HSPA5
FDFT1
FANCD2
DPP4
CAG Drug
CAG
FRGs

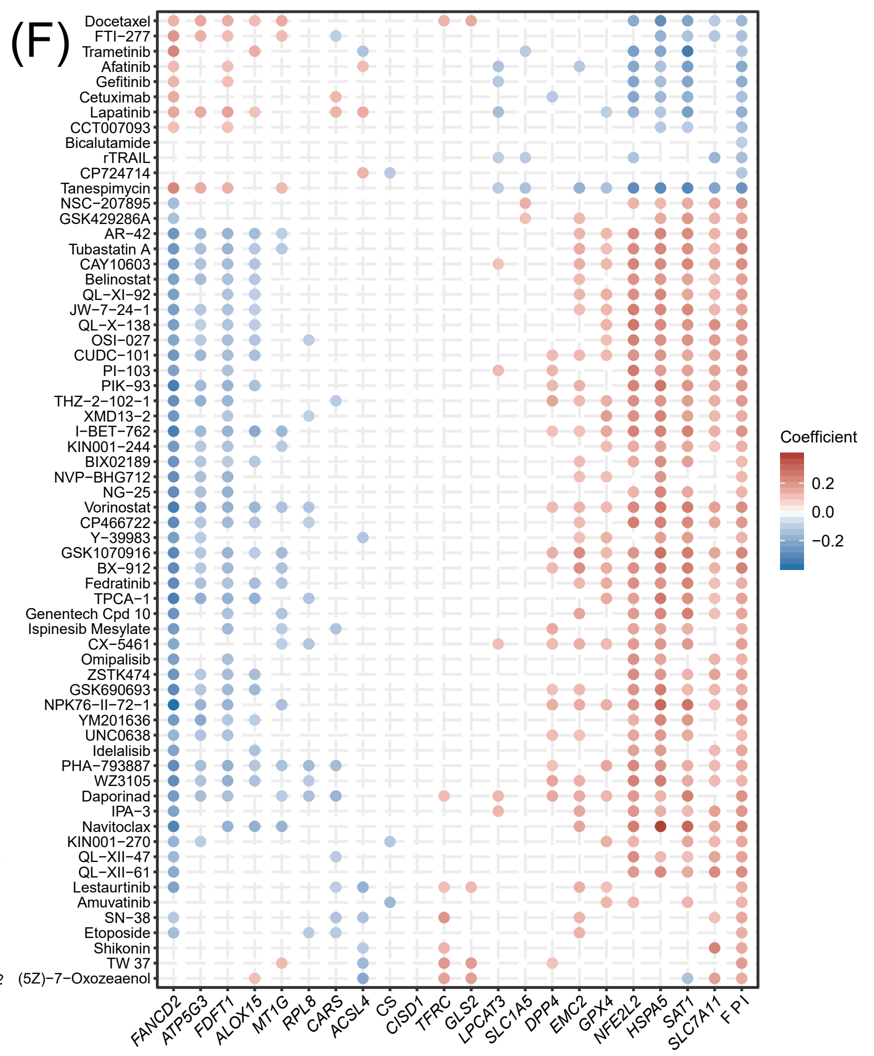
(F)
Docetaxel
FTI−277
Trametinib
Afatinib
Gefitinib
Cetuximab
Lapatinib
CCT007093
Bicalutamide
rTRAIL
CP724714
Tanespimycin
NSC−207895
GSK429286A
AR−42
Tubastatin A
CAY10603
Belinostat
QL−XI−92
JW−7−24−1
QL−X−138
OSI−027
CUDC−101
PI−103
PIK−93
THZ−2−102−1
XMD13−2
I−BET−762
KIN001−244
BIX02189
NVP−BHG712
NG−25
Vorinostat
CP466722
Y−39983
GSK1070916
BX−912
Fedratinib
TPCA−1
Genentech Cpd 10
Ispinesib Mesylate
CX−5461
Omipalisib
ZSTK474
GSK690693
NPK76−II−72−1
YM201636
UNC0638
Idelalisib
PHA−793887
WZ3105
Daporinad
IPA−3
Navitoclax
KIN001−270
QL−XII−47
QL−XII−61
Lestaurtinib
Amuvatinib
SN−38
Etoposide
Shikonin
TW 37
(5Z)−7−Oxozeaenol
FANCD2
ATP5G3
FDFT1
ALOX15
MT1G
RPL8
CARS
ACSL4
CS
CISD1
TFRC
GLS2
LPCAT3
SLC1A5
DPP4
EMC2
GPX4
NFE2L2
HSPA5
SAT1
SLC7A11
FPI
Coefficient
0.2
0.0
−0.2

Figure S4. The pharmacogenomic interaction of the FPI and FRGs. Related to Figure 4.

(A) The co-expression of FRGs and 136 drug-targeted genes. (B) The number of CAGs correlated with FRGs. (C) The number of FRG-CAG correlation pairs. (D) The co-expression of FRGs and 20 genes for immunotherapy. (E) The interactions between drugs, drug targets and FRGs. (F) The correlation between the expression of FRGs and the area under the dose-response curve (AUCs) for drugs.

Transparent Methods

Datasets and Source

The mRNA expression data, copy number alteration thresholded data, masked copy number segmentation data, and DNA methylation 450K data of twenty cancers, including bladder urothelial carcinoma (BLCA), breast invasive carcinoma (BRCA), cholangiocarcinoma (CHOL), colon adenocarcinoma (COAD), cervical and endocervical cancers (CESC), esophageal carcinoma (ESCA), glioblastoma multiforme (GBM), head and neck squamous cell carcinoma (HNSC), kidney chromophobe (KICH), kidney renal clear cell carcinoma (KIRC), kidney renal papillary cell carcinoma (KIRP), liver hepatocellular carcinoma (LIHC), lung adenocarcinoma (LUAD), lung squamous cell carcinoma (LUSC), pancreatic adenocarcinoma (PAAD), prostate adenocarcinoma (PRAD), rectum adenocarcinoma (READ), stomach adenocarcinoma (STAD), thyroid carcinoma (THCA), uterine corpus endometrial carcinoma (UCEC), which had both tumors and normal samples were downloaded from Firehose (http://gdac.broadinstitute.org). Mutation data, miRNA-seq data, and clinical data were downloaded from the Xena Browser (https://xenabrowser.net/datapages/). Additional gene-centric RMA-normalized gene expression profiles and drug response data of over 1000 cancer cell lines were accessed from the Genomics of Drug Sensitivity in Cancer (GDSC) database (https://www.cancerrxgene.org/downloads) (Yang et al., 2013). Immune associated data, including immune cell type fractions and immunophenoscore were obtained from TCIA (https://tcia.at/home) (Charoentong et al., 2017), dysfunction and exclusion scores of tumor samples were obtained from TIDE (http://tide.dfci.harvard.edu/) (Fu et al., 2020; Jiang et al., 2018). Integrated protein-protein interaction data was obtained from the Human Protein Reference Database (http://www.hprd.org/) and BioGRID (https://thebiogrid.org) (Keshava Prasad et al., 2009; Peri et al., 2003). We obtained clinically actionable genes (CAGs) from a previous study (Van Allen et al., 2014) (https://software.broadinstitute.org/cancer/cga/target).

Differential expression analysis of mRNA

To test genes differentially expressed between tumor and normal tissue, gene expression data for 20502 genes across 20 cancer types were downloaded from TCGA at FireBrowse (http://gdac.broadinstitute.org, 2016 January). Then, the fold change and adjusted *P*-value were calculated by the edgeR package (Robinson et al., 2010). We defined genes with an adjusted *P*-value

less than 0.05 as the differential expression genes (DEGs).

Establishing the Ferroptosis Potential Index Model

The index to represent the ferroptosis level was establish based on the expression data for genes of ferroptosis core machine including positive components of *LPCAT3*, *ACSL4*, *NCOA4*, *ALOX15*, *GPX4*, *SLC3A2*, *SLC7A11*, *NFE2L2*, *NOX1*, *NOX3*, *NOX4*, *NOX5* and negative components of *FDFT1*, *HMGCR*, *COQ10A*, *COQ10B*. The enrichment score (ES) of gene set that positively or negatively regulated ferroptosis was calculated using single sample gene set enrichment analysis (ssGSEA) in the R package 'GSVA' (Hanzelmann et al., 2013), and the normalized differences between the ES of the positive components minus negative components was defined as the ferroptosis potential index (FPI) to computationally dissect the ferroptosis levels/trends of the tissue samples.

Somatic Copy-number Alteration (SCNA) and Mutation Analysis

The heterozygosity and homozygosity of amplification and deletion were included to elevate the copy-number alteration of each gene, in which over five percent was regarded as high-frequency SCNA. Pearson's correlation between expression values and copy number segment values of each gene was calculated to evaluate the association between SCNA and expression. The R package "DISCOVER" was employed to evaluate mutual exclusivity between FRGs and tumor suppressor genes or oncogenes across tumor samples in each cancer type (Canisius et al., 2016). The mutation and CNA events were integrated, while only homozygous amplification and deletion were included, and only protein-coding mutations were retained. For each cancer type, the genes were considered to be mutually exclusive if they had a q value of 0.05.

DNA methylation analysis

The R package "IlluminaHumanMethylation-450kanno.ilmn12.hg19" from Bioconductor was imported to annotate the methylation probe for the promoter of each gene. Differential methylation of each gene in tumor and normal samples was tested by the Wilcoxon signed rank test, and genes that were significantly hypomethylated or hypermethylated were identified using a *P*-value cutoff of 0.05. Pearson's correlation between the transcriptional expression of FRGs and the Beta value of the promoter DNA methylation were calculated and considered significant if the *P*-value < 0.05.

miRNA expression analysis

To investigate the mechanisms of dysregulation for ferroptosis regulator genes in cancer, we searched potential miRNAs which might regulate the FRGs based on miRNA-target intersections in starBase. The Spearman correlation between the expression of miRNA and FRGs was statistically evaluated (adjusted *P*-value < 0.1, rho < -0.1). Cytoscape software was used to visualize the high-frequency interaction networks among FRGs and miRNA (Shannon et al., 2003).

Multivariate Regression Analysis of Gene Expression

To assess which factors had significant effects on FRG expression, the expression of each FRG was modeled by linear regression as a function of the median miRNA expression, the median Beta value of promoter methylation, and the copy number of the genes.

Clinical Features Analysis

The R package “survival” was used to assess the prognosis potential of the FRGs and ferroptosis potential index among cancers. For survival analysis, the expression threshold was exhaustively tested and the one with most significant *P*-value was considered the best cut-off. To test the association between ferroptosis level and clinical features, the Pearson correlation was calculated between FPI and tumor stages, age, body mass index (BMI) and cigarette exposure per day, which were converted to numeric variables (“stage1” = 1, “stage2” = 2, etc.). Wilcoxon rank sum tests and Tukey’s tests were used to determine the impact on the ferroptosis potential index for other clinical characteristics including race, remission status, and alcohol. The influence of different MSI statuses(Liu et al., 2018), histologic types, and molecular subtypes on FPI were also considered(Ciriello et al., 2015).

Immune Features Analysis

To study the relationship of ferroptosis and immune microenvironments, we computed the Pearson correlation between FPI and immune parameters including immune cell fractions and 5 types of immunophenoscores.

Identifying the FPI associated significant driver gene mutation

A total of 375 driver genes identified in previous pan-cancer research were included for analysis(Lawrence et al., 2013). To test whether a driver gene's mutational status was significantly associated with ferroptosis among cancers, the rank-transformed FPI was modeled by linear regression as a function of the driver gene's mutational status, ignoring the synonymous variant. To diminish the confounding effects, the rank-transformed count of the total nonsynonymous mutations and the tumor type, which were encoded as virtual variables, were included. To further characterize each cancer, the Benjamini-Hochberg method was used to correct the *P* values across 375 genes. Genes with an adjusted *P* value less than 0.05 for mutation status variable were significantly associated with FPI.

Gene Set Enrichment Analysis

To identify the pathways associated with ferroptosis, the samples of each tumor type were divided into two groups according to the FPI, consisting of the top 30% and bottom 30%. Then, the gene set enrichment analysis (GSEA) was performed (Subramanian et al., 2005).

Correlation between Drug Sensitivity and FPI/FRG Expression

To test the correlation between small molecular drugs and FPI and FRGs, the Pearson correlation coefficients for FPI, the expression value of FRGs and the area under the dose-response curve (AUCs) values were calculated, the results with $|R| > 0.1$ and P-value < 0.05 were considered as significantly correlated. To further investigate the influence of drugs on ferroptosis, the significant association between the expression of clinically actionable genes and FRGs were finished across cancer cell lines, and the associations were filtered with PPIs. Then the drugs which target CAGs were selected according to DrugBank (Wishart et al., 2018) (https://www.drugbank.ca).

Supplemental References

Canisius, S., Martens, J.W., and Wessels, L.F. (2016). A novel independence test for somatic alterations in cancer shows that biology drives mutual exclusivity but chance explains most co-occurrence. Genome Biol *17*, 261.

Charoentong, P., Finotello, F., Angelova, M., Mayer, C., Efremova, M., Rieder, D., Hackl, H., and Trajanoski, Z. (2017). Pan-cancer Immunogenomic Analyses Reveal Genotype-Immunophenotype Relationships and Predictors of Response to Checkpoint Blockade. Cell Rep *18*, 248-262.

Ciriello, G., Gatza, M.L., Beck, A.H., Wilkerson, M.D., Rhie, S.K., Pastore, A., Zhang, H., McLellan, M., Yau, C., Kandoth, C.*, et al.* (2015). Comprehensive Molecular Portraits of Invasive Lobular Breast Cancer. Cell *163*, 506-519.
Fu, J., Li, K., Zhang, W., Wan, C., Zhang, J., Jiang, P., and Liu, X.S. (2020). Large-scale public data reuse to model immunotherapy response and resistance. Genome Med *12*, 21.
Hanzelmann, S., Castelo, R., and Guinney, J. (2013). GSVA: gene set variation analysis for microarray and RNA-seq data. BMC Bioinformatics *14*, 7.
Jiang, P., Gu, S., Pan, D., Fu, J., Sahu, A., Hu, X., Li, Z., Traugh, N., Bu, X., Li, B.*, et al.* (2018). Signatures of T cell dysfunction and exclusion predict cancer immunotherapy response. Nat Med *24*, 1550-1558.
Keshava Prasad, T.S., Goel, R., Kandasamy, K., Keerthikumar, S., Kumar, S., Mathivanan, S., Telikicherla, D., Raju, R., Shafreen, B., Venugopal, A.*, et al.* (2009). Human Protein Reference Database--2009 update. Nucleic Acids Res *37*, D767-772.
Lawrence, M.S., Stojanov, P., Polak, P., Kryukov, G.V., Cibulskis, K., Sivachenko, A., Carter, S.L., Stewart, C., Mermel, C.H., Roberts, S.A.*, et al.* (2013). Mutational heterogeneity in cancer and the search for new cancer-associated genes. Nature *499*, 214-218.
Liu, Y., Sethi, N.S., Hinoue, T., Schneider, B.G., Cherniack, A.D., Sanchez-Vega, F., Seoane, J.A., Farshidfar, F., Bowlby, R., Islam, M.*, et al.* (2018). Comparative Molecular Analysis of Gastrointestinal Adenocarcinomas. Cancer Cell *33*, 721-735 e728.
Peri, S., Navarro, J.D., Amanchy, R., Kristiansen, T.Z., Jonnalagadda, C.K., Surendranath, V., Niranjan, V., Muthusamy, B., Gandhi, T.K., Gronborg, M.*, et al.* (2003). Development of human protein reference database as an initial platform for approaching systems biology in humans. Genome Res *13*, 2363-2371.
Robinson, M.D., McCarthy, D.J., and Smyth, G.K. (2010). edgeR: a Bioconductor package for differential expression analysis of digital gene expression data. Bioinformatics *26*, 139-140.
Shannon, P., Markiel, A., Ozier, O., Baliga, N.S., Wang, J.T., Ramage, D., Amin, N., Schwikowski, B., and Ideker, T. (2003). Cytoscape: a software environment for integrated models of biomolecular interaction networks. Genome Res *13*, 2498-2504.
Subramanian, A., Tamayo, P., Mootha, V.K., Mukherjee, S., Ebert, B.L., Gillette, M.A., Paulovich, A., Pomeroy, S.L., Golub, T.R., Lander, E.S.*, et al.* (2005). Gene set enrichment analysis: a knowledge-based approach for interpreting genome-wide expression profiles. Proc Natl Acad Sci U S A *102*, 15545-15550.
Van Allen, E.M., Wagle, N., Stojanov, P., Perrin, D.L., Cibulskis, K., Marlow, S., Jane-Valbuena, J., Friedrich, D.C., Kryukov, G., Carter, S.L.*, et al.* (2014). Whole-exome sequencing and clinical interpretation of formalin-fixed, paraffin-embedded tumor samples to guide precision cancer medicine. Nat Med *20*, 682-688.
Wishart, D.S., Feunang, Y.D., Guo, A.C., Lo, E.J., Marcu, A., Grant, J.R., Sajed, T., Johnson, D., Li, C., Sayeeda, Z.*, et al.* (2018). DrugBank 5.0: a major update to the DrugBank database for 2018. Nucleic Acids Res *46*, D1074-D1082.
Yang, W., Soares, J., Greninger, P., Edelman, E.J., Lightfoot, H., Forbes, S., Bindal, N., Beare, D., Smith, J.A., Thompson, I.R.*, et al.* (2013). Genomics of Drug Sensitivity in Cancer (GDSC): a resource for therapeutic biomarker discovery in cancer cells. Nucleic Acids Res *41*, D955-961.